HHS Public Access

Author manuscript

Mol Cell. Author manuscript; available in PMC 2020 December 19.

Published in final edited form as:

Mol Cell. 2019 December 19; 76(6): 857–871.e9. doi:10.1016/j.molcel.2019.09.007.

γ-6-phosphogluconolactone, a byproduct of the oxidative pentose phosphate pathway, contributes to AMPK activation through inhibition of PP2A

Xue Gao[1,4,14], **Liang Zhao**[1,4,9,14], **Shuangping Liu**[1,4,10,14], **Yuancheng Li**[2,4], **Siyuan Xia**[1,4], **Dong Chen**[1,4], **Mei Wang**[1,4,11], **Shaoxiong Wu**[3], **Qing Dai**[5], **Hieu Vu**[6], **Lauren Zacharias**[6], **Ralph DeBerardinis**[6], **Esther Lim**[7], **Christian Metallo**[7], **Titus J. Boggon**[8], **Sagar Lonial**[1,4], **Ruiting Lin**[1,4], **Hui Mao**[2,4], **Yaozhu Pan**[1,12], **Changliang Shan**[1,13], **Jing Chen**[1,4,15]

[1]Department of Hematology and Medical Oncology, Emory University School of Medicine, Atlanta, GA 30322, USA.

[2]Department of Radiology and Imaging Sciences, Emory University School of Medicine, Atlanta, GA 30322, USA.

[3]Department of Chemistry, Emory University School of Medicine, Atlanta, GA 30322, USA.

[4]Winship Cancer Institute, Emory University School of Medicine, Atlanta, GA 30322, USA.

[5]Department of Chemistry and Institute for Biophysical Dynamics, University of Chicago, Chicago, Illinois 60637, USA.

[6]UT Southwestern Medical Center, Dallas, TX 75390, USA.

[7]Department of Bioengineering, University of California, San Diego, La Jolla, CA 92093, USA.

[8]Department of Pharmacology, Yale University School of Medicine, New Haven, Connecticut 06520, USA.

[9]Current address: Department of Hematology, Xiangya Hospital, Central South University, Changsha, Hunan 410008, China.

[10]Current address: Department of Pathology, Medical College, Dalian University, Dalian 116622, China.

[15]Lead Contact: jchen@emory.edu (J.C.).

AUTHOR CONTRIBUTIONS

X.G., L. Zhao, S. Liu, and C.S. designed and performed experiments, and analyzed data. Y.L., S.X., D.C., M.W., S.W., F.C., L.Zacharias, R.D., E.L., C.M., M.H., and Y.P., performed experiments, and analyzed data. Q.D. provided crucial study materials and reagents. T.J.B. performed structural analysis and analyzed data. S. Lonial, R.L., and J.C. supervised studies. X.G. and J.C. designed experiments, analyzed data, and wrote the manuscript.

DECLARATION OF INTERESTS

The authors declare no competing interests.

SUPPLEMENTAL INFORMATION

Supplemental information includes seven figures.

[11]Current address: Department of Pharmacy, Children's Hospital of Soochow University, Suzhou 215000, China.

[12]Current address: Department of Hematology, Lanzhou General Hospital, Lanzhou 730050, China.

[13]Current address: State Key Laboratory of Medicinal Chemical Biology, College of Pharmacy and Tianjin Key Laboratory of Molecular Drug Research, Nankai University, Tianjin 300350, China.

[14]These authors contributed equally.

SUMMARY

The oxidative pentose phosphate pathway (oxiPPP) contributes to cell metabolism through not only the production of metabolic intermediates and reductive NADPH, but also inhibition of LKB1-AMPK signaling by ribulose-5-phosphate (Ru-5-P), the product of the third oxiPPP enzyme 6-phosphogluconate dehydrogenase (6PGD). However, we found that knockdown of glucose-6-phosphate dehydrogenase (G6PD), the first oxiPPP enzyme, did not affect AMPK activation despite decreased Ru-5-P and subsequent LKB1 activation, due to enhanced activity of PP2A, the upstream phosphatase of AMPK. In contrast, knockdown of 6PGD or 6-phosphogluconolactonase (PGLS), the second oxiPPP enzyme, reduced PP2A activity. Mechanistically, knockdown of G6PD or PGLS decreased or increased 6-phosphogluconolactone level, respectively, which enhanced the inhibitory phosphorylation of PP2A by Src. Furthermore, γ-6-phosphogluconolactone, an oxiPPP byproduct with unknown function generated through intramolecular rearrangement of δ-6-phosphogluconolactone, the only substrate of PGLS, bound to Src and enhanced PP2A recruitment. Together, oxiPPP regulates AMPK homeostasis by balancing the opposing LKB1 and PP2A.

eTOC Blurb

"Dead end" metabolites in the metabolic reaction network do not have known metabolic functions. In this article, Gao et al. report that γ-6PGL, a byproduct of the oxiPPP, contributes to the Src-PP2A-AMPK signaling pathway by binding to Src and consequently enhancing PP2A recruitment, suggesting that "dead end" metabolites may function as signaling molecules.

Graphical Abstract

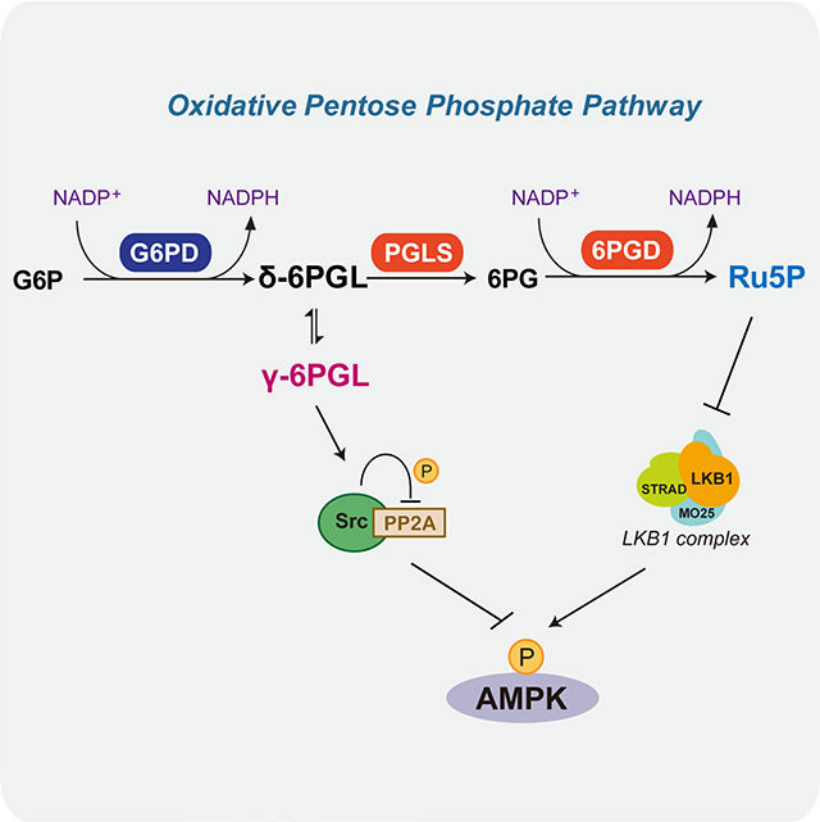

INTRODUCTION

Oncogenic mutations alter cellular metabolism to coordinate bioenergetics, anabolic biosynthesis and appropriate redox status, which provide an overall metabolic advantage to cancer cell proliferation and tumor development (Cairns et al., 2011; Kroemer and Pouyssegur, 2008; Vander Heiden et al., 2009). However, the interplay between metabolic pathways and cell signaling networks remains largely unknown. Besides the “long-term” genomic regulation of metabolic enzymes involving gene expression, oncogenic signals “reprogram” cancer cells in an “acute” manner involving diverse post-translational modifications (PTMs) of metabolic enzymes including tyrosine phosphorylation and lysine acetylation (Hitosugi and Chen, 2014). For example, 6-phosphogluconate dehydrogenase (6PGD), the third enzyme in the oxidative pentose phosphate pathway (oxiPPP) is commonly lysine-acetylated and activated both in normal cells stimulated by EGF, and in cancer cells transformed by oncogenic tyrosine kinases (Lin et al., 2015; Shan et al., 2014). In addition, metabolites can function not only as “building blocks” for macromolecule biosynthesis and cell proliferation but also as signaling molecules to allow novel crosstalk among metabolic pathways and between metabolic and signaling networks. For example, glycolytic metabolites 3-phosphoglycerate and 2-phosphoglycerate were reported to inhibit 6PGD and activate phosphoglycerate dehydrogenase in the serine biosynthesis pathway, respectively, to coordinate glycolysis and anabolic biosynthesis in cells (Hitosugi et al., 2012). Thus, studies of the interplay between metabolic and cell signaling networks are

informative not only to advance our understanding of complex but precise regulatory mechanisms through which oncogenic signals coordinate metabolic and cellular processes to promote tumorigenesis and tumor growth, but also to provide therapeutic insights into the clinical treatment of cancer.

During glycolysis, glucose-6-phosphate can be diverted into the oxiPPP, which produces ribose-5-phosphate (R-5-P) and/or nicotinamide adenine dinucleotide phosphate (NADPH) (Kroemer and Pouyssegur, 2008). There are three key enzymes along the oxiPPP. Glucose-6-phosphate dehydrogenase (G6PD), the first enzyme of the oxidative PPP, converts glucose-6-phosphate (G-6-P) to 6-phosphogluconolactone (6PGL) and produces NADPH. The second enzyme in the oxiPPP, 6-phosphogluconolactonase (PGLS), converts 6PGL to 6-phosphogluconate (6PG). The third enzyme in the pathway, 6PGD, converts 6PG to ribulose-5-phosphate (Ru-5-P) and produces NADPH. The final product of the oxiPPP, R-5-P, is the building block for nucleotide synthesis, while NADPH not only fuels macromolecular biosynthesis such as lipogenesis, but also functions as a crucial antioxidant to quench the reactive oxygen species (ROS) produced during rapid proliferation of cancer cells, which is important for the maintenance of cellular redox homeostasis. Therefore, the oxidative PPP plays a crucial role in the metabolic coordination of glycolysis, biosynthesis and redox homeostasis in cells.

Indeed, attenuation of 6PGD activity in cancer cells inhibits cell proliferation and tumor growth. This is due in part to reduced levels of 6PGD products ribulose-5-phosphate and NADPH, which leads to reduced RNA and lipid biosynthesis as well as elevated ROS (Lin et al., 2015; Shan et al., 2014). Moreover, Ru-5-P functions as a signaling molecule that allows crosstalk between the oxiPPP and lipogenesis pathway. 6PGD activates lipogenesis through controlling its product Ru-5-P, which inhibits the LKB1-AMPK pathway by disrupting the active LKB1 complex, leading to activation of acetyl-CoA carboxylase 1 (ACC1) (Lin et al., 2015). However, cellular responses to the targeting of the first oxiPPP enzyme, G6PD, in cancer cells have been controversial. Knockdown of G6PD leads to attenuated cell proliferation in cancer cells such as human melanoma A375 and leukemia THP-1 cells (Li et al., 2009; Xu et al., 2016), but not in lung cancer H1299 cells (Lin et al., 2015), suggesting that G6PD-related metabolic and cellular functions may vary in cancer cells due to different cell types or oncogenic backgrounds.

The product of G6PD, 6-phosphogluconolactone, was initially believed to be unstable and hydrolyzes spontaneously to form 6-phosphogluconate (Jarori and Maitra, 1991; Miclet et al., 2001). Nuclear magnetic resonance (NMR) spectroscopy studies revealed two different forms of 6-phosphogluconolactone, δ-6-phosphogluconolactone (δ-6PGL) and γ-6-phosphogluconolactone (γ-6PGL), in the G6PD reaction (Jarori and Maitra, 1991). Further studies indicated that δ-6PGL is the only product of G6PD and the sole substrate of the subsequent PGLS in the oxiPPP, while γ-6PGL is generated by intramolecular rearrangement of δ-6PGL. Moreover, although δ-6PGL and γ-6PGL can be converted to each other, only δ-6PGL can undergo spontaneous hydrolysis to form 6PG, whereas γ-6PGL is relatively stable and represents a “dead end” byproduct that does not participate in the oxiPPP (Miclet et al., 2001). In cells, the hydrolysis of δ-6PGL is accelerated by PGLS to form 6PG, which not only represents an important step in the oxiPPP but also

prevents accumulation of γ-6PGL (Miclet et al., 2001). However, the physiological function of γ-6PGL as a byproduct of the oxiPPP remains unknown. Herein, we report an important regulatory function of γ-6PGL in AMPK activation through inhibition of its upstream phosphatase PP2A.

RESULTS

Knockdown of G6PD does not affect AMPK activation despite decreased Ru-5-P and subsequent LKB1 activation

We found that knockdown of G6PD did not alter the phosphorylation levels of AMPK and ACC1 in diverse human cancer cells (Figure 1A), whereas knockdown of 6PGD resulted in increased phosphorylation levels of AMPK and ACC1 in cancer cells (Figure 1B; (Lin et al., 2015; Shan et al., 2014)). Similar results were obtained using human lung cancer H1299 cells with stable depletion of G6PD or 6PGD by CRISPR/Cas9 (Figure 1C). Consistently, knockdown of 6PGD but not G6PD resulted in a decreased lipogenesis rate in H1299 and human leukemia K562 cells (Figure 1D), despite decreased intracellular levels of Ru-5-P (Figure 1E) in both 6PGD and G6PD knockdown cells. In addition, LKB1 immunoprecipitates from both G6PD and 6PGD knockdown K562 cells demonstrated increased kinase activity in an *in vitro* kinase assay using purified recombinant AMPK (rAMPK) as an exogenous substrate (Figure 1F). Moreover, knockdown of G6PD or 6PGD in K562 cells resulted in increased active LKB1 complex formation assessed by increased MO25 association detected in LKB1 immunoprecipitates (Figure 1G). Therefore, knockdown of the first enzyme in the oxiPPP, G6PD, decreases Ru-5-P production and consequently activates LKB1 but does not alter phosphorylation levels of AMPK in cancer cells, suggesting an opposing mechanism that neutralizes AMPK phosphorylation by LKB1 in G6PD knockdown cells.

G6PD knockdown leads to activation of AMPK upstream phosphatase PP2A

We next examined whether G6PD knockdown affects PP2A, which is the upstream phosphatase of AMPK (Joseph et al., 2015). Knockdown of G6PD or 6PGD resulted in increased or decreased PP2A phosphatase activity, respectively, in H1299 and K562 cells (Figure 1H). Consistent with this finding, knockdown of G6PD (Figure 1I, *left*) or 6PGD (Figure 1I, *right*) resulted in decreased or increased inhibitory Y307 phosphorylation levels of PP2A, respectively, in H1299 and K562 cells. In addition, depletion of G6PD or 6PGD by CRISPR/Cas9 also resulted in increased PP2A activity with decreased Y307 phosphorylation (Figure 1J, *left*), or decreased PP2A activity with increased Y307 phosphorylation (Figure 1J, *right*), respectively, in H1299 cells. Moreover, knockdown of PP2A in K562 cells with stable knockdown of G6PD resulted in increased AMPK phosphorylation (Figure 1K) with reduced cell proliferation (Figure 1L). These results suggest that G6PD knockdown activates PP2A to neutralize activated LKB1-AMPK signaling.

Two groups of cancer cells exhibit distinct responses to G6PD knockdown due to differential expression levels of mitochondrial superoxide dismutase 2 (SOD2) and consequent ROS alterations

We found that knockdown of G6PD had no effect on cell proliferation rates of cancer cells including lung cancer H1299 and A549, leukemia K562 and KG1a, breast cancer MDA-MB-231, and prostate cancer DU145 cells (Group I; Figure 2A, *left*), but reduced cell proliferation rates of cancer cells including colorectal cancer HT29, WiDr and HCT116, head and neck cancer Tu686 and Tu212, breast cancer MCF7 and MDA-MB-468, and prostate cancer PC3 cells (Group II; Figure 2A, *right*), despite knockdown of G6PD having no effect on AMPK activation in any of the tested cancer cells (Figure 1A). This difference in response might be due to that G6PD knockdown significantly elevated ROS levels in Group II cells but not in Group I cells (Figure 2B). We found that the mRNA and protein levels of SOD2 are commonly and significantly higher in Group I cells compared to those in Group II cells (Figure 2C–2D, respectively), whereas protein expression levels of other ROS-scavenging enzymes including SOD1, TRX2, GSR, CAT and PRX3 as well as ROS-producing NOX4 are comparable in Group I and II cells (Figure 2D). Moreover, G6PD knockdown resulted in further increased SOD2 protein levels in diverse Group I cells but not in Group II cells, while expression levels of other ROS-scavenging or -producing enzymes remain unaltered in Group I and II cells upon G6PD knockdown (Figure 2E). Furthermore, knockdown of SOD2 converts Group I cells to “Group II-like” cells that are sensitive to G6PD knockdown with decreased cell proliferation and increased ROS levels (Figure 2F and S1A). In contrast, overexpression of SOD2 converts Group II cells to “Group I-like” cells that are resistant to G6PD knockdown with unaltered cell proliferation and ROS levels (Figure 2G and S1B). These data suggested that further increased expression of the ROS-scavenging SOD2 protects the Group I cells from decreased $NADPH/NADP^+$ upon G6PD knockdown, whereas this mechanism does not exist in Group II cells.

In a xenograft experiment where nude mice were injected with parental Group I H1299 cells or cells with G6PD depleted by CRISPR/Cas9, no significant changes were observed in tumor growth rate, tumor mass, ROS levels, AMPK and ACC1 phosphorylation levels (Figure 3A) or cell proliferation assessed by Ki67 expression levels detected by immunohistochemistry staining (Figure S1C) between tumors derived from G6PD depleted cells and control H1299 cells, despite significantly decreased Y307 phosphorylation and phosphatase activity levels of PP2A in G6PD depleted xenograft tumors compared to control tumors (Figure 3A; *right two panels*). In contrast, knockdown of G6PD in Group II HT29 cells resulted in decreased tumor growth rate, tumor mass (Figure 3B, *left two panels*) and Ki67 expression levels (Figure S1D) with increased ROS levels (Figure 3B, *middle panel*) but unaltered AMPK and ACC1 phosphorylation levels, despite significantly decreased Y307 phosphorylation and phosphatase activity levels of PP2A in xenograft tumors of G6PD knockdown compared to control tumors (Figure 3B, *right two panels*).

Consistently, treatment with an antioxidant agent N-acetylcysteine (NAC) did not alter cell proliferation rates of Group I H1299 and K562 parental and G6PD knockdown cells (Figure 3C) but significantly rescued the decreased cell proliferation rates in Group II HT29 and WiDr cells with stable knockdown of G6PD (Figure 3D). In addition, stable knockdown of

G6PD sensitized Group I K562 (Figure S1E), H1299 and DU145 cells (Figure S1F) as well as Group II HT29 and WiDr cells (Figure S1G) to treatment with AMPK activator A769662 (Choudhury et al., 2014; Hadad et al., 2014) in terms of inhibition of cell proliferation. In contrast, knockdown of 6PGD resulted in decreased cell proliferation in both Group I and II cells (Figure S2A–S2B, respectively). Depletion of 6PGD but not G6PD by CRISPR/Cas9 decreased the cell proliferation potential of H1299 cells (Figure S2C), and lysates of xenograft tumors derived from H1299 cells with 6PGD depletion by CRISPR/Cas9 showed increased AMPK and ACC1 phosphorylation with reduced PP2A activity accompanied with increased Y307 phosphorylation (Figure S2D). However, knockdown of G6PD or 6PGD in Group I or II cells showed similar patterns in terms of decreased oxiPPP flux rate, NADPH/$NADP^+$ ratio, and RNA biosynthesis rate (Figure S3E–S3G, respectively) and increased glycolytic rate, lactate production, and intracellular ATP levels (Figure S3H–S3J, respectively). Thus, these results together suggest that the differential ROS levels in response to G6PD knockdown in Group I and II cells likely determine the different cell proliferation responses upon G6PD knockdown.

Knockdown of PGLS, the second enzyme in the oxiPPP, inhibits PP2A but activates LKB1, leading to consequent activation of AMPK with increased ROS

To determine which step in the oxiPPP contributes to PP2A regulation, we next examined the role of the second enzyme in the oxiPPP, PGLS (Figure 4A) in cancer cell metabolism and tumor growth. We found that stable knockdown of PGLS in Group I H1299 and K562 cells as well as Group II HT29 and WiDr cells resulted in increased phosphorylation levels of AMPK and ACC1 (Figure 4B) with decreased cell proliferation rates and increased ROS levels (Figure 4C–4D, respectively). In addition, knockdown of G6PD but not PGLS or 6PGD resulted in increased mRNA levels of SOD2 in Group I cells (Figure 4E), whereas G6PD knockdown did not alter the mRNA levels of SOD2 in Group II cells (Figure 4F). Moreover, knockdown of G6PD but not PGLS increased SOD2 protein levels in Group I cells, but did not alter protein levels of other SOD-scavenging or –producing enzymes (Figure S3A). These data together suggest that depletion of G6PD but not PGLS promotes SOD2 expression to quench ROS in Group I cells.

Consistent with these findings, LKB1 immunoprecipitates from PGLS knockdown K562 cells showed increased kinase activity in an *in vitro* LKB1 kinase assay using rAMPK as an exogenous substrate (Figure 4G) with increased active LKB1 complex formation assessed by increased protein amount of co-immunoprecipitated MO25 (Figure 4H). In addition, PGLS knockdown resulted in decreased PP2A phosphatase activity with increased inhibitory Y307 phosphorylation of PP2A in H1299 and K562 cells (Figure 4I–4J, respectively). These results are consistent with decreased reduced oxiPPP flux rates (Figure S3B) and lipogenesis rates (Figure S3C, *left*), as well as increased glycolysis and ATP levels in PGLS knockdown cells (Figure S3C, *middle* and *right,* respectively). In a xenograft experiment in which nude mice were injected with control H1299 cells or PGLS knockdown cells, the growth rate and masses of tumors (Figure S3D, *left two panels*) derived from PGLS knockdown cells were significantly reduced with decreased expression of the cell proliferation marker Ki-67 assessed by immunohistochemical staining (Figure S3D, *middle panel*), increased ROS levels and phosphorylation levels of AMPK and ACC1 with decreased PP2A phosphatase

activity (Figure S3D, *right three panels*), compared to those of tumors formed by control cells.

We next examined the effect of reductive agent NAC and/or AMPK inhibitor Compound C on cell proliferation and tumor growth potential of H1299 cells with PGLS knockdown. We found that stable knockdown of PGLS resulted in decreased cell proliferation of H1299 cells compared to parental cells, while single agent treatment with NAC or Compound C only partially rescued the reduced cell proliferation of H1299 cells with PGLS knockdown (Figure 4K, *left* and *middle, respectively*). In contrast, combined treatment with NAC and Compound C completely rescued the decreased cell proliferation of H1299 cells with PGLS knockdown (Figure 4K, *right*) by reducing both ROS and AMPK activation (Figure 4L), suggesting that both ROS and AMPK activation contribute to reduced cell proliferation upon PGLS knockdown. Similar results were obtained using a xenograft mouse model of tumor. Compared to tumors derived from parental H1299 cells, stable knockdown of PGLS resulted in decreased tumor growth potential of H1299 cells in mice (Figure S3E, *left*) with reduced tumor sizes (Figure 4M, *left* and S3E, *upper middle*), increased ROS and AMPK phosphorylation levels (Figure 4M, *middle* and S3E, *lower middle,* respectively), and reduced cell proliferation potential assessed by IHC staining of Ki67 (Figure 4M, *right* and S3E, *right*). Consistently, single agent treatment with NAC or Compound C only partially rescued the reduced tumor growth rates and sizes, reduced the increased ROS or AMPK phosphorylation levels, and increased the reduced Ki67 staining in tumor derived from H1299 cells with PGLS knockdown, whereas combined treatment with NAC and Compound C almost completely reversed these phenotypes in PGLS knockdown tumors (Figure 4M and S3E).

In *LKB1 null* A549 and DU145 cancer cells, PGLS knockdown resulted in decreased cell proliferation (Figure S4A) with increased ROS levels (Figure S4B). We observed unaltered AMPK phosphorylation in DU145 cells but a slight increase in AMPK phosphorylation in A549 cells (Figure S4C), which might be due to the decreased PP2A activity upon PGLS knockdown. Interestingly, NAC treatment completely reversed the reduced cell proliferation potential of DU145 cells, but only achieved partial rescue in A549 cells, upon PGLS knockdown (Figure S4D). Consistently, CRISPR-mediated knockout of PGLS but not G6PD resulted in reduced cell proliferation in A549 cells (Figure S5A), while treatment with NAC partially rescued the reduced cell proliferation of A549 cells with PGLS knockout (Figure S5B). In contrast, treatment with Compound C did not alter cell proliferation of A549 cells with PGLS knockout (Figure S5B). Similar results were obtained using a xenograft mouse model of tumor. Compared to tumors derived from parental A549 cells, stable knockout of PGLS resulted in decreased growth potential of tumors derived from A549 cells in mice with reduced tumor sizes (Fig S5C), increased ROS levels and slightly increased AMPK phosphorylation (Figure S5D), and reduced cell proliferation potential assessed by IHC staining of Ki67 (Figure S5E). Treatment with NAC partially rescued the aforementioned phenotypes in tumors derived from PGLS KO A549 cells, whereas Compound C had no effects on basal activation levels of AMPK (Figure S5D, *right*), or cell proliferation and tumor growth potential of A549 cells that are LKB1-deficient despite expression levels of PGLS (S5B and S5C, respectively). These data suggest that PGLS deficiency attenuates cell

proliferation in A549 cells partially through an unknown mechanism independent of AMPK and PP2A, in addition to increased ROS levels.

Taken together, knockdown of PGLS in cancer cells resulted in similar phenotypes as knockdown of 6PGD (Lin et al., 2015) but not G6PD, suggesting that the step between G6PD and PGLS in the oxiPPP is crucial for PP2A regulation.

6-phosphogluconolactone, product of G6PD and substrate of PGLS, enhances inhibitory phosphorylation of PP2A by Src

We thus examined the role of 6PGL in PP2A-AMPK signaling since 6PGL is the metabolic intermediate between G6PD and PGLS in the oxiPPP (Figure 5A, *upper panel*). Indeed, knockdown of G6PD resulted in decreased 6PGL levels in H1299 cells, while knockdown of PGLS or 6PGD led to 6PGL accumulation (Figure 5A, *lower left*). In contrast, knockdown of G6PD or PGLS resulted in decreased 6PG level, whereas knockdown of 6PGD resulted in increased 6PG level in H1299 cells (Figure 5A, *lower right*).

We next produced 6PGL by incubating G6P with purified rG6PD, and removing rG6PD from the reaction mixture at the production endpoint. Since 6PGL spontaneously hydrolyzes to form 6PG (Jarori and Maitra, 1991; Miclet et al., 2001), we terminated the reaction prior to completion and the resulting product mixture was spectrophotometrically measured to contain about 8.5 mM G6P, 1.3 mM 6PG, and 200 μM 6PGL. We found that adding an increasing concentration of 6PGL product mixture to K562 cell lysates resulted in increased Y307 phosphorylation of PP2A (Figure 5B), whereas incubation with increasing concentrations of purchased purified 6PG, the hydrolysis product of 6PGL did not affect PP2A phosphorylation (Figure 5C). In addition, control experiments revealed that incubation with purchased purified G6P and/or 6PG at the concentrations representing those of G6P and 6PG, respectively, in the 6PGL product mixture used in Figure 5B did not affect PP2A phosphorylation (Figure S6A–S6C), suggesting that 6PGL was the functional component in the mixture that regulates PP2A phosphorylation.

Moreover, knockdown of G6PD in K562 cells resulted in decreased Y307 phosphorylation of PP2A with increased PP2A activity but unaltered AMPK phosphorylation, which were reversed by rescuing the decreased 6PGL levels in the cell lysates, leading to increased AMPK activation (Figure 5D). In contrast, knockdown of 6PGD in K562 cells resulted in increased Y307 phosphorylation of PP2A with decreased PP2A activity and consequently increased AMPK phosphorylation due to increased 6PGL levels, which were further enhanced by adding additional 6PGL in the cell lysates (Figure 5E). Moreover, knockdown of PP2A resulted in increased AMPK phosphorylation in K562 cells with stable knockdown of G6PD, which could not be reversed by rescuing the decreased 6PGL (Figure 5F).

Tyrosine kinase Src inhibits PP2A through Y307 phosphorylation (Chen et al., 1994). We found that knockdown of G6PD or 6PGD in K562 cells resulted in decreased or increased association between Src and PP2A, respectively (Figure 5G). In addition, incubation of immunoprecipitated Src with purified recombinant PP2A (rPP2A) in the presence of increasing concentrations of 6PGL resulted in elevated Y307 phosphorylation levels of PP2A (Figure 5H) with increased PP2A binding to Src (Figure 5I). In contrast, G6P and/or

6PG controls at the concentrations in the 6PGL product mixture used in Figure 5H did not affect Src-dependent phosphorylation of PP2A (Figure S6D–S6F). These data together suggest that 6PGL but not G6P or 6PG promotes Src and PP2A association, leading to increased PP2A phosphorylation.

γ-6PGL, an oxiPPP byproduct generated through intramolecular rearrangement of δ-6PGL, the physiological substrate of PGLS, enhances inhibition of PP2A by Src

We next determined whether δ-6PGL and/or γ-6PGL (Figure 6A) enhances Src-dependent phosphorylation and inhibition of PP2A. Similar to total 6PGL levels (Figure 5A), NMR studies revealed that knockdown of G6PD decreased the intracellular levels of δ-6PGL in H1299 cells, whereas knockdown of PGLS or 6PGD elevated δ-6PGL levels (Figure 6B, *left*). Similarly, knockdown of G6PD resulted in significantly decreased γ-6PGL from approximately 11.8μM to 1.2μM, while knockdown of PGLS or 6PGD caused accumulation of γ-6PGL (Figure 6B, *right*).

We next purified the synthesized γ-6PGL converted from 6PG and δ-6PGL synthesized from D-glucono-1.5-lactone. Incubation of immunoprecipitated Src with rPP2A in the presence of increasing concentrations of purified synthesized γ-6PGL but not δ-6PGL resulted in elevated Y307 phosphorylation levels of PP2A (Figure 6C), whereas neither γ-6PGL nor δ-6PGL altered immunoprecipitated Src-dependent phosphorylation of recombinant focal adhesion kinase (rFAK), an alternative Src substrate (Figure 6D), or phosphorylation of myelin basic protein (MBP), a nonspecific Src substrate (Figure 6E). In addition, incubation with increasing concentrations of γ-6PGL but not δ-6PGL resulted in increased PP2A binding to the immunoprecipitated Src (Figure 6F), whereas neither γ-6PGL nor δ-6PGL altered protein-protein interaction between FAK and immunoprecipitated Src (Figure 6G). These data together suggest that γ-6PGL selectively promotes Src and PP2A association and subsequent PP2A phosphorylation.

γ-6PGL binds to Src and enhances PP2A recruitment

We sought to examine whether γ-6PGL binds to Src and/or PP2A to promote their protein-protein interaction. We found that ^{14}C-labeled 6PGL but not ^{14}C-labeled G6P binds to purified Src, whereas neither ^{14}C-labeled 6PGL nor G6P binds to purified PP2A (Figure S6G). In addition, in a thermal shift assay, incubation with purified γ-6PGL but not δ-6PGL resulted in shift in a melting temperature of purified rSrc (Figure 7A, *left two panels,* respectively), suggesting a direct interaction between γ-6PGL and Src, whereas neither γ-6PGL nor δ-6PGL incubation affected melting temperature of purified rPP2A (Figure 7A, *right two panels,* respectively). This is consistent with the finding that both γ-6PGL and δ-6PGL had no direct effect on PP2A phosphatase activity using purified rPP2A in an *in vitro* PP2A phosphatase assay (Figure S6H). In addition, although the purity of synthesized γ-6PGL is approximately 50%, compensating with reaction substrate 6PG, control melting temperature thermal shift experiment excluded the possibility of purified 6PG binding to rSrc (Figure S7A). To map out the region(s) on Src that mediates binding of γ-6PGL and/or PP2A, we generated a group of truncated constructs of Src (Figure S7B). We found that PP2A is able to bind multiple regions of Src including SH3 and SH2 domains as well as the

C-terminal catalytic domain (Figure S7C), whereas γ-6PGL only binds to the catalytic domain (Figure 7B and S7D).

Furthermore, purified rSrc pre-incubated with increasing concentrations of γ-6PGL but not δ-6PGL demonstrated enhanced binding activity to purified rPP2A (Figure 7C), whereas pre-incubation with either γ-6PGL or δ-6PGL did not alter the ability of PP2A to interact with rSrc (Figure 7D). In addition, rSrc pre-treated with γ-6PGL but not δ-6PGL showed enhanced kinase activity to phosphorylate rPP2A at Y307 (Figure 7E). Only the constructs containing the catalytic domain of Src demonstrated increasing ability to interact with PP2A in the presence of increasing concentrations of γ-6PGL (Figure 7F and S7E). These results together suggest that γ-6PGL but not δ-6PGL selectively binds to the catalytic domain of Src to enhance PP2A recruitment as a Src substrate.

DISCUSSION

Our results reveal a dual role of the oxiPPP in the regulation of AMPK activation through balancing the opposing upstream kinase Src and phosphatase PP2A (Figure 7G). The byproduct γ-6PGL converted from δ-6PGL branches out of the oxiPPP to promote Src-dependent inhibition of PP2A by binding to Src and subsequently enhancing PP2A recruitment, while a further downstream oxiPPP intermediate, Ru-5-P, inhibits LKB1 by disrupting the active LKB1 complex (Figure 7G; (Lin et al., 2015)). During the oxiPPP, δ-6PGL, when produced by G6PD, is quickly hydrolyzed by PGLS, preventing not only the accumulation of δ-6PGL but also subsequent intramolecular rearrangement to form γ-6PGL (Miclet et al., 2001). Thus, it is likely that in cancer cells, the oxiPPP flux rate is commonly elevated, leading to relatively low levels of γ-6PGL to sustain basal level activity of PP2A but relatively high levels of Ru-5-P that inhibit LKB1, which act in concert to maintain a low level of AMPK activation that allows activation of ACC1 and subsequently lipogenesis, providing both metabolic and proliferative advantages to tumor growth. Thus, these findings reveal additional crosstalk between the oxiPPP and LKB1-AMPK signaling pathway, showcasing the complex crosstalk between metabolic and cellular signaling networks that allows precisely controlled and coordinated regulation of cellular processes.

We identified γ-6PGL, previously considered a “dead end” byproduct of the oxiPPP with unknown physiological function, as a signaling molecule that links the metabolic oxiPPP with the Src-PP2A-AMPK signaling pathway. This finding suggests that, although dead end metabolites including γ-6PGL as well as so called “metabolic wastes” such as creatinine and uric acid, which are produced by metabolic reactions but cannot be metabolically consumed, represent “dead ends” in the metabolic reaction network and do not have metabolic functions (Mackie et al., 2013; Zamir and Devor, 1987), they may function as signaling molecules that allow crosstalk between different metabolic pathways within the metabolic signaling network, or between metabolic pathways and the cellular signaling network. Future studies are warranted to comprehensively advance our understanding of the metabolic and/or signaling roles of metabolites including “dead end” metabolites.

γ-6PGL and δ-6PGL can be converted to each other (Miclet et al., 2001). When G6PD is knocked down, production of δ-6PGL is reduced, which might promote conversion from

γ-6PGL to δ-6PGL, which can be further hydrolyzed by PGLS. This may explain the decreased γ-6PGL levels in G6PD knockdown cells. When PGLS or 6PGD is knocked down, δ-6PGL accumulates, allowing the formation of γ-6PGL that accumulates to much higher levels compared to δ-6PGL. This might be due to the fact that γ-6PGL does not spontaneously hydrolyze (k= 0 min^{-1}) and that the conversion rate constant of δ-6PGL to γ-6PGL (k= 0.028 min^{-1}) is higher than that of the reverse conversion (k= 0.021 min^{-1}). Moreover, the spontaneous hydrolysis of δ-6PGL (k= 0.010 min^{-1}) is slower compared to the intramolecular rearrangement of δ-6PGL to form γ-6PGL (k= 0.028 min^{-1}) (Miclet et al., 2001). That being said, intrinsically δ-6PGL could form γ-6PGL more quickly than being hydrolyzed to form 6PG. Therefore, PGLS is required to accelerate hydrolysis of δ-6PGL to form 6PG in cells to avoid accumulation of γ-6PGL, suggesting that PGLS activity is crucial to control δ-6PGL and γ-6PGL levels, in addition to the 6PGL-producing G6PD. Human PGLS activity was reported to be 3,330 units/mg (Miclet et al., 2001). Therefore, in human cells, the equilibriums between γ-6PGL and δ-6PGL, as well as δ-6PGL and its hydrolysis product 6PG, depend on the amount of PGLS and concentrations of δ-6PGL. Our detection of both δ-6PGL and γ-6PGL by NMR in human tumor cells further confirms the intracellular co-existence and equilibrium of δ-6PGL and γ-6PGL in live cells.

How PGLS is regulated remains unknown, however. We reported that lysine acetylation activates 6PGD (Shan et al., 2014), and other groups also reported that tyrosine phosphorylation and lysine acetylation activates and inhibits G6PD, respectively (Liu et al., 2019; Wang et al., 2014). Thus, PGLS could be similarly regulated through post-translational modifications. Future studies are warranted to decipher the mechanisms by which PGLS is regulated under different physiological conditions that may affect, for example, post-translational modification levels of PGLS, and how the interplay between activities of G6PD and PGLS contributes to the equilibrium between γ-6PGL and δ-6PGL.

Our findings suggest that γ-6PGL binds to Src and selectively enhances PP2A recruitment as a substrate, but it does not affect recruitment of other substrates such as FAK. Our results also suggest that PP2A as a substrate binds to the SH3 and SH2 domains of Src in addition to the catalytic domain, which is consistent with the notion that the catalytic domains of tyrosine kinases may not solely determine the substrate specificity (reviewed in (Miller, 2003)). Catalytic tyrosine kinase domains need to coordinate with other non-catalytic domains (such as SH3 and SH2 domains) to determine which substrates to bind to, recruit and present to the catalytic domains. Since our results showed that γ-6PGL does not affect FAK as a Src substrate binding to Src, our findings suggest a novel mechanism by which γ-6PGL binds to the catalytic domain of Src and coordinates with the SH3 and SH2 domains to selectively facilitate the recruitment and presentation of PP2A as a substrate to Src. Future studies are warranted to elucidate the detailed molecular and structural mechanisms underlying γ-6PGL-binding dependent enhancement of Src-PP2A association.

Our results also suggest an important role for G6PD as the first enzyme in the oxiPPP to not only channel the glycolytic metabolite G6P into the oxiPPP and consequently initiate and sustain the oxiPPP flux, but also coordinate with other oxiPPP enzymes to balance the opposing LKB1 and PP2A to “fine tune” the activation of AMPK in order to achieve

optimized cell survival and proliferation. We showed that the oxiPPP flux rates were decreased to comparable extents with increased glycolytic rate and decreased NADPH/$NADP^+$ ratios when knocking down individual G6PD, PGLS or 6PGD in diverse cells, meaning that the overall flux passing through the pathway is reduced upon knockdown of each oxiPPP enzyme, despite the other oxiPPP enzymes retaining their protein and activity levels. The overall reduced oxiPPP flux in G6PD, PGLS or 6PGD knockdown cells might redirect glucose-6-phosphate to glycolysis, leading to increased glycolytic rate and ATP levels. The decreased NADPH/$NADP^+$ ratios in cells with individual knockdown of G6PD, PGLS or 6PGD reflects the overall effect of the decreased oxiPPP flux on NADPH that cannot be compensated by other NADPH producing enzymes including IDH1 and ME1.

Responses to G6PD attenuation may vary among cancer cells, depending on the differential expression levels of ROS-scavenging SOD2. Future studies are warranted to explore the signaling and molecular mechanisms as well as the cellular and genetic basis by which G6PD regulates SOD2 gene expression only in Group I cancer cells. In addition, some cancer cell lines such as human lung cancer A549 cells were reported to show decreased cell proliferation rate upon G6PD knockdown (Hsieh et al., 2013), whereas stable knockdown of G6PD did not alter the cell proliferation rate of A549 cells in the current study. This difference may be due to cell heterogeneity, or to isolated experimental conditions applied such as different G6PD knockdown efficiencies.

STAR★METHODS

CONTACT FOR REAGENT AND RESOURCE SHARING

Further information and requests for resources and reagents should be directed to and will be fulfilled by Jing Chen (jchen@emory.edu).

EXPERIMENTAL MODEL AND SUBJECT DETAILS

Animal study—Animal experiments were conducted and designed according to protocols approved by the Institutional Animal Care and Use Committee of Emory University. Nude mice (athymic nu/nu, female 4–6weeks old, Harlan Laboratories) were used for xenograft studies.

Cell lines—HEK293T, DU145, MDA-MB-231, MCF7, and MDA-MB-468 cells were cultured in Dulbecco Modified Eagle Medium (DMEM) with 10% fetal bovine serum (FBS). H1299, A549, K562, and KG-1a cells were cultured in RPMI 1640 medium with 10% FBS. HCT116, HT29 and WiDr cells were cultured in McCoy's 5a medium with 10% FBS. PC3, Tu212 and Tu686 cells were cultured in DMEM/F12 medium with 10% FBS. All the cells were cultured at 37°C and 5% CO_2.

METHOD DETAILS

Lentivirus production and stable knockdown cell lines construction—To construct cell lines with stable knockdown endogenous G6PD, 6PGD, PGLS, and PP2A, lentivirus carrying shRNA were generated. Briefly, to produce lentivirus, lentiviral vector harboring shRNA, psPAX2 packaging plasmid, and pMD2.G envelope plasmid (Addgene)

were co-transfected into HEK293T cells using TransIT®-LT1 Transfection Reagent (Mirus Bio) according to the manufacturer's instructions. Fresh medium was changed 24 hours later and lentivirus-containing supernatant medium was collected 48 hours after transfection. To construct stable knockdown cells, target cells were infected with harvested lentivirus-containing supernatant for 24 hours and selected with 2μg/mL puromycin. Knockdown efficiency was confirmed by western blot.

CRISPR/Cas9 depletion—H1299 cells with G6PD or 6PGD depleted by CRISPR/Cas9, and A549 cells with G6PD or PGLS depleted by CRISPR/Cas9, were constructed described previously (Sanjana NE, Shalem O, Zhang F. Nature Methods, 2014). The G6PD and 6PGD sgRNAs were designed on this website: (http://portals.broadinstitute.org/gpp/public/analysis-tools/sgrna-design) and cloned into the lentiCRISPRv2 vector backbone. The PGLS sgRNA was purchased from GenScript (SC1678). LentiCRISPRv2 vector harboring sgRNA, psPAX2 packaging plasmid, and pMD2.G envelope plasmid (Addgene) were co-transfected into HEK293T cells using TransIT®-LT1 Transfection Reagent (Mirus Bio) according to the manufacturer's instructions to produce lentivirus. Fresh medium was changed 24 hours later and lentivirus-containing supernatant medium was collected 48 hours after transfection. H1299 or A549 cells were infected with harvested lentivirus-containing supernatant for 24 hours and then selected with 2μg/mL puromycin for cells with stable G6PD, PGLS, and 6PGD individual depletion by CRISPR/Cas9. Depletion efficiency was confirmed by western blot. Please also see detailed information related to shRNA sequence, sgRNA sequence, plasmids names, and reagents information in KEY RESOURCES TABLE.

siRNA Transfection and RNA Interference—For RNA interference experiments, *siSOD2* (SI03060498 and SI03025652) and control siRNA (1022076) were purchased from Qiagen. All siRNA transfection experiments were performed with Lipofectamine® RNAiMAX Transfection Reagent (13778030, Life Technologies). Cells were seeded for cell proliferation assay 24 hours after transfection. Cells were harvested for western blot 72 hours after transfection to check the knockdown efficiency. Please also see detailed information in KEY RESOURCES TABLE.

Transient transfection—pcDNA3.1-FLAG-SOD2 (OHu19808D, GenScript) was transfected using Lipofectamine® 3000 (L3000015, Life Technologies) according to the manufacturer's instructions. Cells were seeded for cell proliferation assay 24 hours after transfection. Cells were harvested for western blot 48 hours after transfection.

Quantitative RT-PCR—RNA was extracted by using TRIzol Reagent (Invitrogen). Quantitative RT-PCR was conducted with PrimeScript™ 1st strand cDNA Synthesis Kit (Takara) and iTaq Universal SYBR Green Supermix (Bio-Rad). Real-time primers targeting *SOD2* and *GAPDH* were obtained from Integrated DNA Technologies (IDT). The Sequence of primers are listed in Key Resources Table.

Cell proliferation assay—Cell proliferation assays were performed by seeding 2–8×10^4 cells in a 6-well plate and culturing at 37°C under normal conditions (5% CO_2 and 95% air). Cell proliferation was determined by cell numbers recorded within 5 days after being seeded and normalized to that of each of the cell lines at the starting time (T=0 hour) by trypan blue

exclusion using TC20 Automated Cell Counter (BioRad). For NAC, A769662 and Compound C treatment, the media was changed every day.

Metabolic assay—For measurement of intracellular reactive oxygen species (ROS) production, 2×10^5 cells were seeded in 6-well plates 24 hours prior to treatment and then treated with 5 μM carboxyH2DCFDA (Invitrogen) for 30min. The cells were harvested, suspended in PBS, and analyzed using a flow cytometer.

Oxidative PPP flux was determined by measuring $^{14}CO_2$ release. Two 6-cm dishes of cells at 80% confluency were prepared. One dish of cells was incubated in 2 mL of medium containing 1-^{14}C-glucose (2 μCi/mL) at 37°C for 4 hours, and the other dish of cells was incubated in 2 ml of medium containing 6-^{14}C-glucose (2 μCi/mL) at 37°C for 4 hours. When treated with labeled glucose, the two dishes of cells were placed in two 10-cm dishes with 2 sealed pinholes, respectively. $^{14}CO_2$ released from cells was collected by sealing the 10-cm dish. The PPP flux was stopped by injecting 0.3 mL of 2N HCl into the cells through one of the holes and released $^{14}CO_2$ was trapped for 12 hours by injecting 0.3 mL of hyamine hydroxide into a cup placed on the 10-cm dish through the second hole. Hyamine hydroxide was dissolved in methanol and directly subjected to scintillation counting. The scintillation count of 6-^{14}C-glucose treatment was subtracted from the scintillation count of 1-^{14}C-glucose treatment, indicating$^{14}CO_2$ released from the PPP flux.

NADPH/$NADP^+$ ratio was detected using $NADP^+$/NADPH Quantitation Colorimetric Kit according to the manufacturer's instructions.

For lipogenesis assay, 8×10^5 cells were seeded in 6-well plates 24 hours prior to treatment and then incubated in complete medium with 2 μCi/mL of D-[U-^{14}C]-glucose for 2 hours. Lipids were extracted by hexane:isopropanol (3:2 v/v), dried, suspended in chloroform, and subjected to scintillation counting. Scintillation counts were normalized to cell numbers.

For RNA biosynthesis assay, 8×10^5 cells were seeded in 6-well plates 24 hours prior to treatment and then incubated in complete medium with 2 μCi/mL of D-[U-^{14}C]-glucose for 2 hours. RNA was extracted using RNeasy columns (Qiagen). ^{14}C-RNA was assayed by scintillation counter and normalized to the amount of total RNA.

For glycolytic rate measurement, 1×10^6 cells were incubated in 1 mL of Krebs buffer without glucose for 30 min at 37°C. The Krebs buffer was then replaced with Krebs buffer containing 10 mM glucose with 10 μCi of H-glucose. Following incubation for 1 hour at 37°C, 50 μL medium were transferred to uncapped PCR tubes containing 50 μl of 2 N HCl. The PCR tube was transferred into 1.5 mL tube. The 1.5 mL tube was sealed for diffusion for 24 hours at 37°C. The amounts of diffused ^3H_2O were determined by scintillation counting and indicated the glycolytic rate.

For lactate production assay, 8×10^5 cells were seeded in 6-well plate 24 hours prior to treatment and then incubated with phenol red-free RPMI medium without FBS for 1 hour at 37°C. The lactate in the medium was assessed using lactate assay kit (Biovision) according to the manufacturer's instructions.

For intracellular ATP concentration measurement, 8×10^5 cells were seeded in 6-well plate 24 hours prior to treatment and then collected for detection using somatic ATP assay kit (Sigma).

Cellular metabolite extraction and measurement—Cellular metabolites were extracted and spectrophotometrically measured as described previously (Lin et al., 2015). In brief, indicated cells were harvested, pelleted, and suspended in a volume of hypotonic lysis buffer (50 mM HEPES [PH 7.0], 2 mM $MgCl_2$, 5 mM KCl, 5 mM DTT) equivalent to 3 times the packed cell pellet volume, followed by sonication. The cell lysates were centrifuged at 4°C for 10 min at maximum speed and the supernatants were applied to Amicon Ultra tubes with 10 KDa cutoff filter (Millipore). The flow-through containing the metabolites was used for measurements. For 6-PG, the flow-through was added in reaction buffer (50 mM Tris-HCl [pH 7.0], 1 mM $MgCl_2$, 0.4 mM $NADP^+$, 10 μg/mL recombinant 6PGD protein). Increase in absorbance at 340 nm from NADPH production was measured by a DU800 spectrophotometer (Beckman Coulter). Recombinant PGLS (final concentration of 10 μg/mL) was added in the reaction to convert the 6PGL to 6PG. Increase in absorbance at 340 nm from NADPH production was measured for 6PGL concentration. Purified 6-PG (Sigma) diluted with hypotonic lysis buffer was used as the standard. Ru-5-P was extracted and spectrophotometrically measured as described previously without modification (Lin et al., 2015).

Xenograft studies—Nude mice were subcutaneously injected with 5×10^6 H1299 cells with stable depletion of G6PD or 5×10^6 HT29 cells with stable knockdown of G6PD or 5×10^6 H1299 cells with stable knockdown of PGLS on the right flank. The corresponding cells harboring empty vector were injected on the left flank. Tumor growth was measured from 7–12 days after inoculation by measurement of two perpendicular diameters and the tumor volume was calculated using the formula $4\pi/3 \times (\text{width}/2) \times (\text{length}/2)$. The tumors were harvested and weighed at the experimental endpoint. For the NAC and/or Compound C rescue experiment, nude mice were subcutaneously injected with 5×10^6 H1299 cells with stable knockdown of PGLS or 5×10^6 A549 cells with stable depletion of PGLS on the right flank, and cells harboring empty vector on the left flank, respectively. 5 days after injection, mice were randomized into four groups: one group received one intraperitoneal injection of the vehicle (100 μL PBS/DMSO 10%) at 4-day intervals, the second group received one intraperitoneal injection of 2 mg/kg Compound C (Compound C was dissolved in PBS/DMSO 10%) at 4-day intervals, the third group were provided drinking water with 10 mg/mL of NAC (Jin et al., 2015) plus one intraperitoneal injection of the vehicle (100 μL PBS/DMSO 10%) at 4-day intervals, and the fourth group were provided drinking water with 10 mg/mL of NAC plus one intraperitoneal injection of 2 mg/kg Compound C. Tumor growth was measured by measurement of two perpendicular diameters, and the tumor volume was calculated using the formula $4\pi/3 \times (\text{width}/2) \times (\text{length}/2)$. The tumors were harvested and weighed at the experimental endpoint. To detect the ROS level of the tumor, fresh tumors were removed from xenograft mice, placed in PBS, minced into small pieces using scissors, and digested with digestion buffer (Accumax@ Stemcell). After digestion, the digestion buffer was neutralized with cell culture media, and the cells were strained through 70 μm cell strainer, followed by washing twice with PBS and cell number counting.

2×10^5 tumor cells were treated with 5 μM carboxyH2DCFDA (Invitrogen) for 30 min, washed with PBS for twice, and then analyzed using a flow cytometer.

Immunoprecipitation—Cell or tumor lysates containing about 1–2mg total protein were incubated with primary antibody for at least 3 hours at 4 °C, followed by incubation with Protein G Sepharose 4 Fast Flow beads for 2 hours. The beads were then washed with 1×TBS for 3 times and eluted with SDS sample buffer for Western blotting analysis.

Measurement of intracellular γ-6PGL and δ-6PGL using ^{31}P-NMR spectroscopy—For sample preparation, the indicated cells were harvested once confluent, pelleted and suspended in a volume of hypotonic lysis buffer (500 mM HEPES [PH 7.0], 2 mM $MgCl_2$, 5 mM KCl, 5 mM DTT, prepared with deuterium oxide) equivalent to 3 times the packed cell pellet volume, followed by sonication. The cell lysates were centrifuged at 4 °C for 10 min at maximum speed and the supernatants were applied to Amicon Ultra tubes with 10 KDa cutoff filter (Millipore). The flow-through metabolites containing γ-6PGL and δ-6PGL were measured by quantitative ^{31}P nuclear magnetic resonance (PNMR) spectroscopy (Bruker Avance III HD 600 MHz spectrometer with a Prodigy Cryogen probe). H_3PO_4 (0.74 M) was added into the sample as internal standard. The ^{31}PNMR spectra were acquired with ^{1}H decoupling and the delay time (d1) set to 10 seconds. The concentrations of metabolites were quantified based on the integrations of corresponding peaks vs H_3PO_4 peak.

Production of 6PGL—6PGL production was achieved by converting glucose-6-phosphate (G6P) in 200 μL reaction buffer (rG6PD protein 5 U(sigma), 10 mM G6P, 5 mM $NADP^+$, 5 mM $MgCl_2$ and 50 mM Tris, pH 7.0) for 5 min at room temperature. The reaction mixture was applied to Amicon Ultra tubes with 10KDa cutoff filter (Millipore) to centrifuge at 4°C for 10 min at 12,000g to remove the enzyme protein. δ-6PGL was produced through this enzymatic method at first. The δ-6PGL was converted to γ-6PGL through intramolecular rearrangement rapidly and hydrolyzed to 6-PG spontaneously (Miclet et al., 2001). The flow-through reaction mixture was spectrophotometrically measured to contain about. 8.5 mM G6P, 1.3 mM 6PG, 100 μM δ-6PGL, and 100 μM γ-6PGL.

Synthesis of γ-6PGL and δ-6PGL

1) Synthesis of 6-delta-PGL (δ-6PGL):

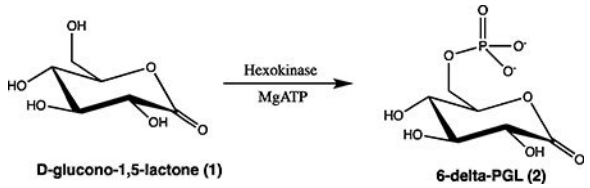

δ-6PGL was synthesized from D-glucono-1.5-lactone (Korczynska et al., 2014). Positive control reaction was carried out to test the activity of the hexokinase enzyme (from Aldrich, 1000 U was shipped as lipolyzed at room temperature, after arrival, 1000 μL water was added to give 1 U/μL). In an NMR tube, 390 μL water, 50 μL MES buffer (1M, pH 6.0), glucose (2 mg) in 20 μL water, MgATP (2 mg in 20 μL water), and 20 μL Hexokinase (20 U)

were added. The mixture was incubated at 30°C and monitored by ^{31}P NMR spectrum. After 1 hour incubation, all the MgATP peaks disappeared and the peaks of ADP were visible. At the same time, the two peaks of G-6-P also showed up at a 2:1 ratio, suggesting that the hexokinase has good activity. To produce δ-6PGL, 290 μL water + 50 μL 1 M MES buffer (6.0) +20 μL MgATP (0.1 mg/μL) + 20 μL D-glucono-1.5-lactone (0.1 mg/ μL) + 120 μL hexokinase enzyme were added in an NMR tube. The mixture was incubated at 30 °C for 3 hours and ^{31}P NMR spectrum showed that besides ATP peaks, there was a new peak formed at 1.3 ppm, corresponding to the desired product δ-6PGL. As a negative control, no product δ-6PGL was formed without adding hexokinase. D-glucono-1.5-lactonewas not a good substrate as glucose, therefore, more hexokinase and longer reaction time were needed.

2) Synthesis of 6-gamma-PGL (γ-6PGL):

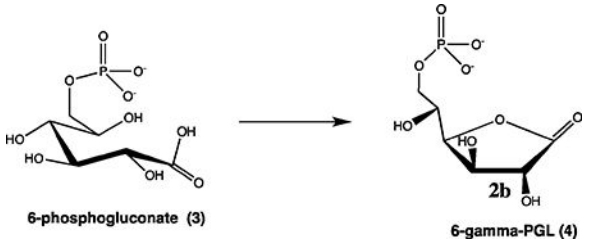

γ-6PGL was synthesized from (6-phosphogluconate) 6-PG. Dowex 50 WX8 resin (H^+ form, 450 mg) in an Eppendorf tube was washed with 2×1 mL 2N HCl and then 3× 1 mL water. 52 mg 6-PG dissolved in 1 mL water was added and rotated at room temperature for 10 min. After centrifugation, theion exchange resin was sedimented and supernatant was transfer to a vial. Theion exchange resin was washed with 2× 1 mL water and supernatants were combined. The vial was immersed in a 50°Coil bath and blown with nitrogen. After drying, 1 mL methoxyethanol was added and the sample dried again by air blowing. After pumping for 15 min, 1 mL DMSO-$d_6$was added and 0.5 mL was removed to conduct ^{13}C NMR spectrum, showing the main peak at 176 ppm, suggesting it is γ-6PGL (Beutler et al., 1986). When stored at −20°C in DMSO for one week, the ^{13}C NMR spectrum showed no change, suggesting γ-6PGL is stable under the storage conditions.

PP2A activity assay—A malachite green-based phosphatase assay kit (Echelon) was used to measure PP2A activity. To determine endogenous PP2A activity, PP2A was immunoprecipitated from the indicated cell lines and tumor tissues with PP2A antibody for at least 3 hours at 4°C, followed by incubation with Protein G Sepharose 4 Fast Flow beads for 2 hours at 4°C. The PP2A-bound beads were washed 3 times with 1×TBS and 2 times with PP2A activity assay buffer (20 mM MOPS [pH 7.5], 60 mM 2-mercaptoethanol, 100 mM NaCl, 0.1 mg/mL BSA), followed by incubation with the substrate, threonine phosphopeptide (amino acid sequence: KRp-TIRR, Millipore) in assay buffer for 1 hour at room temperature. PP2A activity was measured by detecting the free phosphate removed from the substrate by PP2A using malachite green reagent in Malachite Green Assay Kit (Echelon) following the manufacturer's instructions. PP2A activity was normalized to immunoprecipitated PP2A protein level detected by Western blot.

***In vitro* kinase assays—**LKB1 *in vitro* kinase assay was performed as described previously(Lin et al., 2015). In brief, endogenous LKB1 was immunoprecipitated from the indicated K562 stable knockdown cells by LKB1 antibody (Cell Signaling Technologies) and incubated with AMPK substrate in kinase buffer (50 mM Tris [PH 7.5], 10 mM $MgCl_2$, 1 mM DTT, 100 μM ATP) for 20 min at 30°C, followed by SDS-PAGE electrophoresis and western blot detection.

For Src *in vitro* kinase assay, endogenous Src was immunoprecipitated from K562 cells with Src antibody (Cell Signaling Technologies) for 3 hours at 4°C, followed by incubation with Protein G Sepharose 4 Fast Flow beads for 2 hours at 4°C. The Src-bound beads were washed 3 times with 1 × TBS and 2 times with Src kinase assay buffer (60 mM Tris [pH 7.0], 5 mM $MgCl_2$, 0.5 mM $MnCl_2$, 12.5 μM Na_3VO_4, 0.125 mM DTT, 200 μM ATP). Kinase assay was carried out in kinase buffer for 30 min at room temperature, using recombinant 200 ng PP2A or 200 ng FAK or 5 μg MBP as substrates per reaction, in the presence of indicated concentrations of 6PGL or γ-6PGL or δ-6PGL. The reaction mixture was boiled directly with SDS sample buffer and applied to SDS-PAGE electrophoresis and western blot detection of the phosphorylation of the substrates. Alternatively, the reaction mixture was washed with 3 times with 1×TBS to retain the Src-bound beads and then eluted with SDS sample buffer, followed by SDS-PAGE electrophoresis and western blot detection of the substrates binding with Src.

Cell-free system assays—Cell free assays were performed as previously described (Lin et al., 2015). Briefly, the indicated cells were harvested once confluent, pelleted and suspended in a volume of PBS equivalent to 3 times the packed cell pellet volume, followed by sonication. The cell mixture was added to different concentrations of 6PGL or 6PG to reach the final concentrations for 30 min at room temperature with gentle shaking every 5 minutes. After incubation, the mixture was added to equal volume of PBS containing 2% NP40 and inhibitor cocktails. The samples were then centrifuged and the supernatant was used for determination of endogenous PP2A activity as described or for western blot of PP2A and AMPK phosphorylation.

Plasmids construction and Src truncated proteins purification—Truncated *SRC* sequences containing a carboxyl-terminal FLAG tag were obtained by PCR using *SRC* (OHu28514D, GenScript) as a template and cloned into expression vector pDEST53. The full length Src contains amino acids 1–536 followed by a carboxyl-terminal FLAG tag, the SH3 domain contains amino acids 88–143 followed by a carboxyl-terminal FLAG tag, the SH2 domain contains amino acids 147–247 followed by a carboxyl-terminal FLAG tag, the AC domain contains amino acids 1–247 followed by a carboxyl-terminal FLAG tag, the catalytic domain contains amino acids 250–536 followed by a carboxyl-terminal FLAG tag, and the AN domain contains amino acids 88–536 followed by a carboxyl-terminal FLAG tag. To purify proteins, truncated *SRC* constructs were transformed into BL21(DE3) Chemically Competent E. coli (C600003, Invitrogen). The bacteria were inoculated into 250 mL LB medium, incubated until OD_{600} reach to around 0.5–0.9, and subjected to 0.5 mM IPTG-induction for 16 hours at 25°C. Bacteria cell lysates were obtained by centrifugations and sonication, and loaded onto a Ni-NTA column. The bound proteins were eluted and then

desalted using a PD-10 column (GE). To detect truncated Src interaction with PP2A, the desalted truncated Src proteins were immunoprecipitated with ANTI-FLAG M2 Affinity Gel (A2220–5ML, Sigma-Aldrich) and then incubated with purified recombinant human protein PP2A (sigma). The FLAG beads were washed 3 times with 1×TBS [PH 7.0] and eluted with SDS buffer for western blot to check PP2A binding. For thermal melt shift assay, the desalted truncated Src proteins were further purified by immunoprecipitation with ANTI-FLAG M2 Affinity Gel for 3 hours at 4°C and elution with FLAG peptide (F3290–25MG, Sigma-Aldrich). Please also see detailed information in KEY RESOURCES TABLE.

Src and PP2A sequential binding assay—Per reaction, 100 ng of purified recombinant human protein Src (Thermo Fisher Scientific) or PP2A (Sigma) was suspended in 200 μL 1×TBS, followed by incubation for 3 hours at 4°C with Src or PP2A antibody, respectively. 15 μL protein G beads were added into the mixture for further incubation for 2 hours at 4°C. The beads were then washed 3 times with 1×TBS, followed by incubating in 1 × TBS [PH 7.0] for 30 min at room temperature, in the presence of indicated concentrations of γ-6PGL or δ-6PGL. The protein-bound beads were then washed 3 times with 1 × TBS [PH 7.0] to remove the superfluous γ-6PGL or δ-6PGL. Next, 100 ng recombinant PP2A or Src was added to the Src-bound or PP2A-bound beads, respectively. After immunoprecipitation for 30 min at room temperature, the beads were then washed 3 times with 1×TBS [PH 7.0] and eluted with SDS buffer for western blot to check protein binding. Alternatively, after PP2A and Src-bound beads incubation, the reaction mixture was boiled directly with SDS sample buffer and applied to SDS-PAGE electrophoresis and western blot detection of the PP2A phosphorylation. For truncated Src proteins sequential binding assay, the Src truncated proteins were incubated with ANTI-FLAG M2 Affinity Gel for 3 hours at 4°C. The beads were then washed 3 times with 1×TBS, followed by incubating in 1 × TBS [PH 7.0] for 30 min at room temperature, in the presence of indicated concentrations of γ-6PGL. The protein-bound beads were then washed 3 times with 1×TBS [PH 7.0] to remove the superfluous γ-6PGL. Next, 100 ng recombinant PP2A was added to the truncated Src-bound beads. After immunoprecipitation for 30 min at room temperature, the beads were then washed 3 times with 1×TBS [PH 7.0] and eluted with SDS buffer for western blot to check PP2A binding.

Thermal melt shift assay—The thermal melt shift assay was performed as previously described (Hitosugi et al., 2012). Briefly, thermal shift assay of compound-protein interaction was performed in 96-well PCR plates with various compound concentrations and 200ng protein per reaction using protein thermal shift dye kit (Applied Biosystems) according to the manufacturer’s instructions.

Immunohistochemical staining—Ki67 staining was performed as previously described (Kang et al., 2015). In brief, resected tumors from xenograft mice were fixed in 10% buffered formalin, embedded in paraffin and mounted on slides. The tumor sections were deparaffinized, rehydrated, and then incubated in 3% hydrogen peroxide to suppress endogenous peroxidase activity. Antigen retrieval was achieved by microwaving the sections in 10 mM sodium citrate (pH6.0). Sections were then blocked using 10% goat serum. Human Ki67 antibody (Abcam) was applied to the slides at dilution of 1:200 overnight at

4°C. Detection was achieved with the Dako IHC kit (Agilent technologies). Slides were stained with 3,3′-diaminobenzidine, washed, counterstained with hematoxylin, dehydrated, and mounted. Images of each slide were taken using an inverted microscope for data analysis.

Radiometric metabolite-protein binding assay—Labeled 6PGL was produced by converting D-[U-^{14}C]-glucose-6-phosphate (American Radiolabeled Chemicals) as described. Purified GST tagged PP2A (sigma) or His tagged Src (Thermo Fisher Scientific) were pre-bound with GST-beads or His-beads, respectively, followed by incubating with ^{14}C-labeled 6PGL or G6P in 1×TBS (pH 7.0) buffer for 30 min at room temperature. Beads-bound PP2A or Src were washed, eluted, and radioactivity was detected by scintillation counting.

QUANTIFICATION AND STATISTICAL ANALYSIS

A two-tailed Student's *t* test was used to generate *p* values in studies in which statistical analyses were performed, except a two-way ANOVA was used for cell proliferation assay and tumor growth analysis. *p* values less than or equal to 0.05 were considered significant. Data with error bars represent mean ± SD. Statistical analysis and graphical presentation was performed using Prism 5.0 (GraphPad).

DATA AND SOFTWARE AVAILABILITY

All software used in this study is listed in the Key Resources Table.

Supplementary Material

Refer to Web version on PubMed Central for supplementary material.

ACKNOWLEDGMENTS

We thank Dr. Anthea Hammond for critical reading and editing of the manuscript. This work was supported in part by NIH grants CA140515, CA183594, CA174786 (J.C.), National Institutes of Health grant K01 HG006699 (Q.D.), and Joel A. Katz Music Medicine Fund supported by the T.J. Martell Foundation/Winship Cancer Institute (J.C. and R.L.). R.L. is a Special Fellow of The Leukemia & Lymphoma Society. J.C. is the Winship 5K Scholar and the R. Randall Rollins Chair in Oncology.

REFERENCES

Beutler E, Kuhl W, and Gelbart T (1986). Blood cell phosphogluconolactonase: assay and properties. Br J Haematol 62, 577–586. [PubMed: 3954969]

Cairns RA, Harris IS, and Mak TW (2011). Regulation of cancer cell metabolism. Nature reviews. Cancer 11, 85–95. [PubMed: 21258394]

Chen J, Parsons S, and Brautigan DL (1994). Tyrosine phosphorylation of protein phosphatase 2A in response to growth stimulation and v-src transformation of fibroblasts. J Biol Chem 269, 7957–7962. [PubMed: 7510677]

Choudhury Y, Yang Z, Ahmad I, Nixon C, Salt IP, and Leung HY (2014). AMP-activated protein kinase (AMPK) as a potential therapeutic target independent of PI3K/Akt signaling in prostate cancer. Oncoscience 1, 446–456. [PubMed: 25594043]

Hadad SM, Hardie DG, Appleyard V, and Thompson AM (2014). Effects of metformin on breast cancer cell proliferation, the AMPK pathway and the cell cycle. Clin Transl Oncol 16, 746752.

Hitosugi T, and Chen J (2014). Post-translational modifications and the Warburg effect. Oncogene 33, 4279–4285. [PubMed: 24096483]

Hitosugi T, Zhou L, Elf S, Fan J, Kang HB, Seo JH, Shan C, Dai Q, Zhang L, Xie J, et al. (2012). Phosphoglycerate mutase 1 coordinates glycolysis and biosynthesis to promote tumor growth. Cancer Cell 22, 585–600. [PubMed: 23153533]

Hsieh YT, Lin MH, Ho HY, Chen LC, Chen CC, and Shu JC (2013). Glucose-6-phosphate dehydrogenase (G6PD)-deficient epithelial cells are less tolerant to infection by Staphylococcus aureus. PLoS One 8, e79566. [PubMed: 24223971]

Jarori GK, and Maitra PK (1991). Nature of primary product(s) of D-glucose 6-phosphate dehydrogenase reaction. 13C and 31P NMR study. FEBS Lett 278, 247–251. [PubMed: 1991519]

Jin L, Li D, Alesi GN, Fan J, Kang HB, Lu Z, Boggon TJ, Jin P, Yi H, Wright ER, et al. (2015). Glutamate dehydrogenase 1 signals through antioxidant glutathione peroxidase 1 to regulate redox homeostasis and tumor growth. Cancer Cell 27, 257–270. [PubMed: 25670081]

Joseph BK, Liu HY, Francisco J, Pandya D, Donigan M, Gallo-Ebert C, Giordano C, Bata A, and Nickels JT Jr. (2015). Inhibition of AMP Kinase by the Protein Phosphatase 2A Heterotrimer, PP2APpp2r2d. J Biol Chem 290, 10588–10598. [PubMed: 25694423]

Kang HB, Fan J, Lin R, Elf S, Ji Q, Zhao L, Jin L, Seo JH, Shan C, Arbiser JL, et al. (2015). Metabolic Rewiring by Oncogenic BRAF V600E Links Ketogenesis Pathway to BRAF-MEK1 Signaling. Mol Cell 59, 345–358. [PubMed: 26145173]

Kang S, Elf S, Lythgoe K, Hitosugi T, Taunton J, Zhou W, Xiong L, Wang D, Muller S, Fan S, et al. (2010). p90 ribosomal S6 kinase 2 promotes invasion and metastasis of human head and neck squamous cell carcinoma cells. J Clin Invest 120, 1165–1177. [PubMed: 20234090]

Korczynska M, Xiang DF, Zhang Z, Xu C, Narindoshvili T, Kamat SS, Williams HJ, Chang SS, Kolb P, Hillerich B, et al. (2014). Functional annotation and structural characterization of a novel lactonase hydrolyzing D-xylono-1,4-lactone-5-phosphate and L-arabino-1,4-lactone-5-phosphate. Biochemistry 53, 4727–4738. [PubMed: 24955762]

Kroemer G, and Pouyssegur J (2008). Tumor cell metabolism: cancer's Achilles' heel. Cancer Cell 13, 472–482. [PubMed: 18538731]

Li D, Zhu Y, Tang Q, Lu H, Li H, Yang Y, Li Z, and Tong S (2009). A new G6PD knockdown tumor-cell line with reduced proliferation and increased susceptibility to oxidative stress. Cancer Biother Radiopharm 24, 81–90. [PubMed: 19243250]

Lin R, Elf S, Shan C, Kang HB, Ji Q, Zhou L, Hitosugi T, Zhang L, Zhang S, Seo JH, et al. (2015). 6-Phosphogluconate dehydrogenase links oxidative PPP, lipogenesis and tumour growth by inhibiting LKB1-AMPK signalling. Nature Cell Biology 17, 1484–1496. [PubMed: 26479318]

Liu R, Li W, Tao B, Wang X, Yang Z, Zhang Y, Wang C, Liu R, Gao H, Liang J, et al. (2019). Tyrosine phosphorylation activates 6-phosphogluconate dehydrogenase and promotes tumor growth and radiation resistance. Nat Commun 10, 991. [PubMed: 30824700]

Mackie A, Keseler IM, Nolan L, Karp PD, and Paulsen IT (2013). Dead end metabolites--defining the known unknowns of the E. coli metabolic network. PLoS One 8, e75210. [PubMed: 24086468]

Miclet E, Stoven V, Michels PA, Opperdoes FR, Lallemand JY, and Duffieux F (2001). NMR spectroscopic analysis of the first two steps of the pentose-phosphate pathway elucidates the role of 6-phosphogluconolactonase. J Biol Chem 276, 34840–34846. [PubMed: 11457850]

Miller WT (2003). Determinants of substrate recognition in nonreceptor tyrosine kinases. Acc Chem Res 36, 393–400. [PubMed: 12809525]

Shan C, Elf S, Ji Q, Kang HB, Zhou L, Hitosugi T, Jin L, Lin R, Zhang L, Seo JH, et al. (2014). Lysine acetylation activates 6-phosphogluconate dehydrogenase to promote tumor growth. Molecular cell 55, 552–565. [PubMed: 25042803]

Vander Heiden MG, Cantley LC, and Thompson CB (2009). Understanding the Warburg effect: the metabolic requirements of cell proliferation. Science 324, 1029–1033. [PubMed: 19460998]

Wang YP, Zhou LS, Zhao YZ, Wang SW, Chen LL, Liu LX, Ling ZQ, Hu FJ, Sun YP, Zhang JY, et al. (2014). Regulation of G6PD acetylation by SIRT2 and KAT9 modulates NADPH homeostasis and cell survival during oxidative stress. EMBO J 33, 1304–1320. [PubMed: 24769394]

Xu SN, Wang TS, Li X, and Wang YP (2016). SIRT2 activates G6PD to enhance NADPH production and promote leukaemia cell proliferation. Sci Rep 6, 32734. [PubMed: 27586085]

Zamir LO, and Devor KA (1987). Kinetic pulse-labeling study of Fusarium culmorum. Biosynthetic intermediates and dead-end metabolites. J Biol Chem 262, 15348–15353. [PubMed: 3680199]

Research Highlight

- G6PD knockdown activates PP2A to neutralize activated LKB1-AMPK signaling
- G6PD product 6-phosphogluconolactone (6PGL) promotes PP2A inhibition by Src
- γ-6PGL binds to Src and enhances PP2A recruitment
- γ-6PGL as a “dead end” byproduct of oxiPPP has physiological function

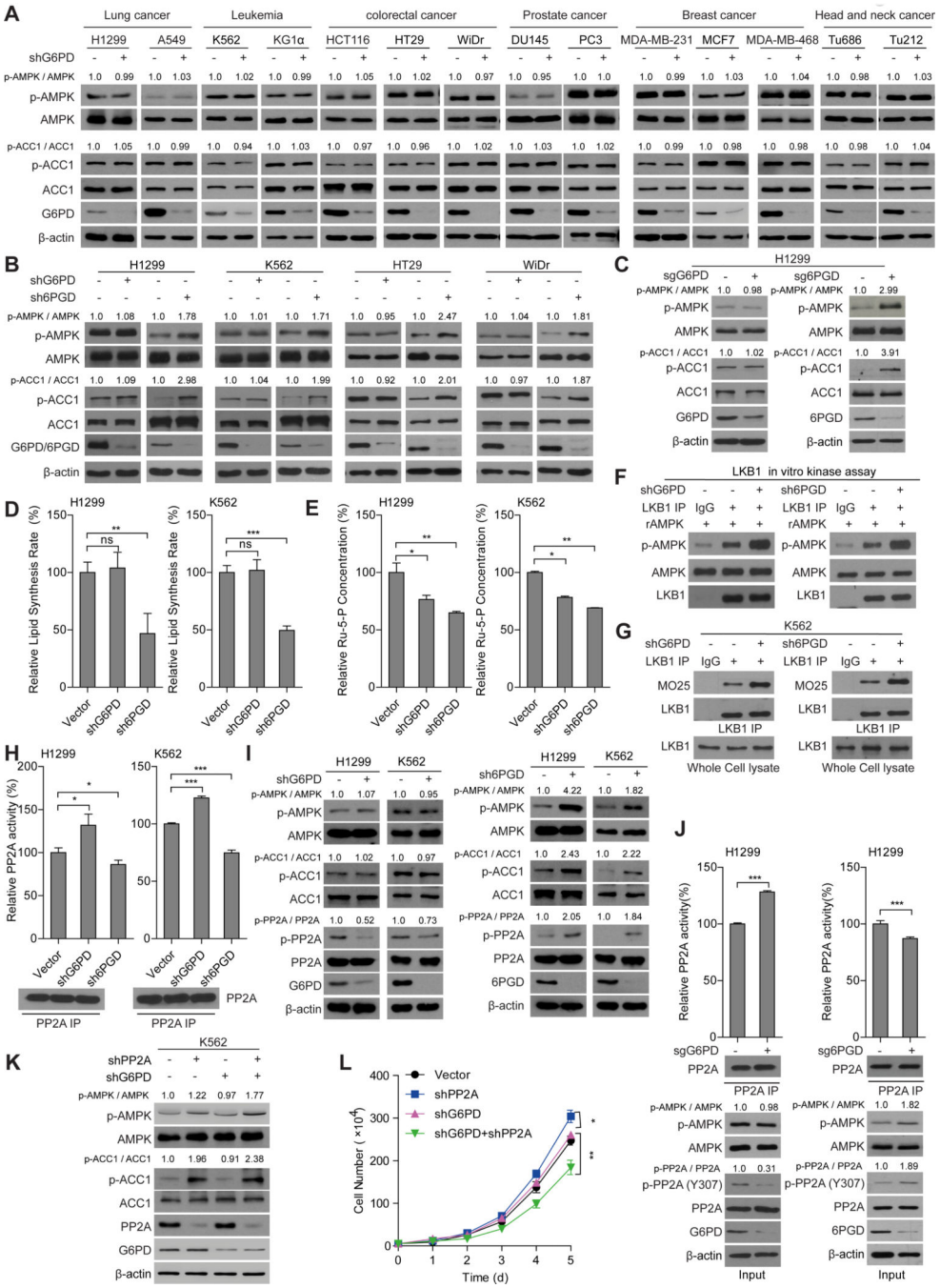

Figure 1. G6PD attenuation activates PP2A to neutralize activated LKB1-AMPK signaling.

(A) Western blot showing effects of G6PD knockdown on AMPK and ACC1 phosphorylation in diverse human cancer cell lines from lung cancer, leukemia, colorectal cancer, prostate cancer, breast cancer and head and neck cancer.

(B) Western blot showing effects of G6PD or 6PGD knockdown on AMPK and ACC1 phosphorylation in representative H1299, K562, HT29 and WiDr cells.

(C) Western blot showing AMPK and ACC1 phosphorylation in H1299 cells with G6PD or 6PGD CRISPR knockout.

(D-E) H1299 cells (*left panels*) and K562 cells (*right panels*) with G6PD or 6PGD stable knockdown were tested for lipogenesis (D) and intracellular level of Ru-5-P (E).
(F) LKB1 precipitated from K562 cells with or without G6PD (*left*) and 6PGD (*right*) knockdown was incubated with recombinant AMPK (rAMPK) in an *in vitro* kinase assay. Western blot showing AMPK phosphorylation by LKB1.
(G) Western blot showing the effect of G6PD (*left*) or 6PGD (*right*) stable knockdown on endogenous LKB1 and MO25 interaction in K562 cells.
(H) Effect of G6PD or 6PGD stable knockdown on PP2A enzyme activity in H1299 (*left*) and K562 (*right*) cells.
(I) Western blot showing effects of G6PD knockdown (*left*) or 6PGD knockdown (*right*) on AMPK, ACC1, and PP2A phosphorylation in H1299 cells and K562 cells.
(J) PP2A enzyme activity (*upper panels*) and phosphorylation levels of both AMPK and PP2A (*lower panels*) were tested in H1299 cells with G6PD (*left*) and 6PGD (*right*) CRISPR knockout.
(K-L) Effect of additional PP2A knockdown on AMPK and ACC1 phosphorylation (K), and cell proliferation rate (L) in K562 cells with G6PD knockdown.
Data are mean ± SD (D, E, H, J and L). *p* values were obtained by a two-tailed Student's *t* test except for a two-way ANOVA test in L (ns, not significant; *0.01 < p < 0.05; **0.001 < p < 0.01; *** p< 0.001).

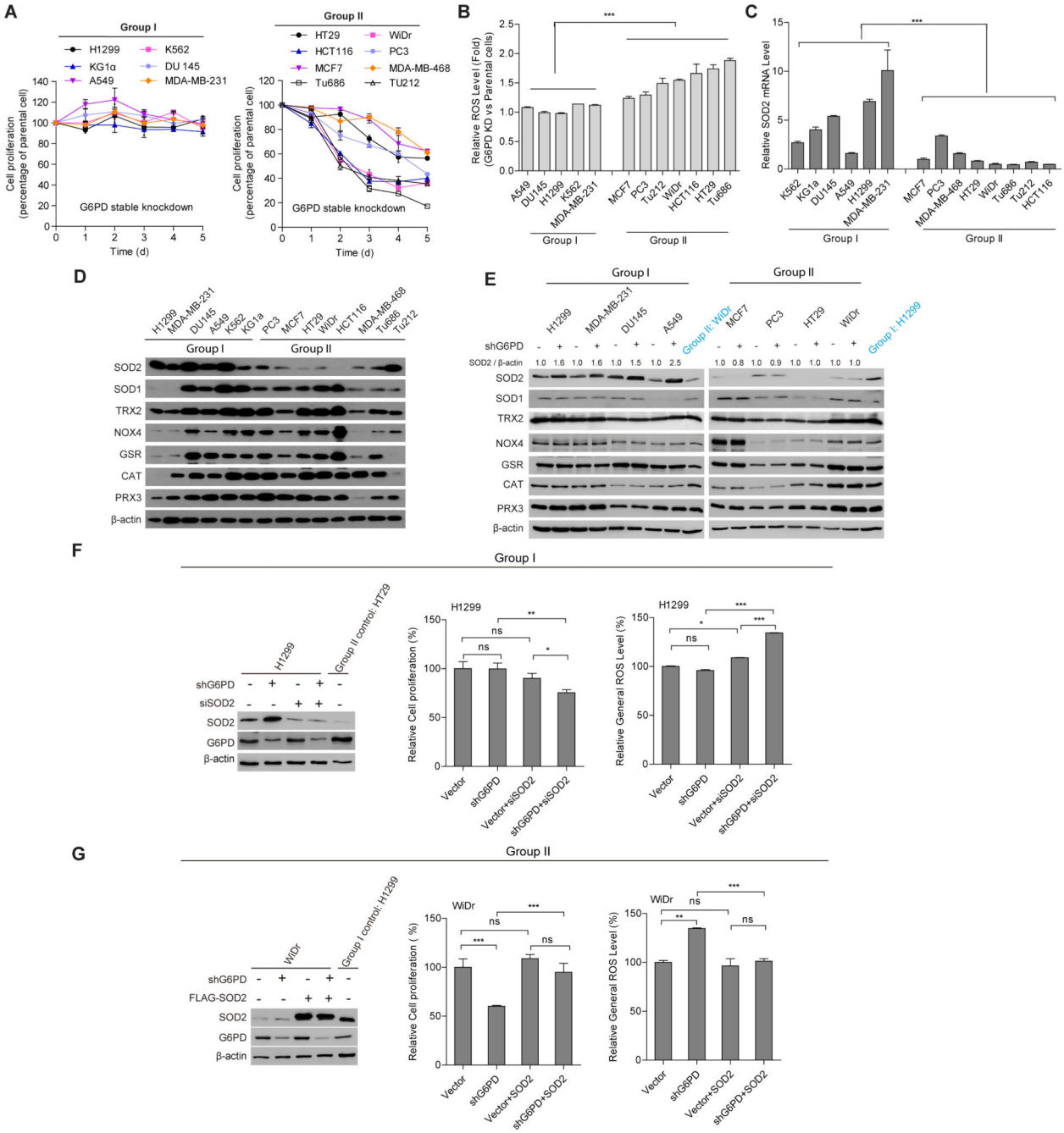

Figure 2. Two groups of cancer cells respond distinctly to G6PD attenuation due to differential SOD2 expression level and consequent ROS alterations.

(A) Cell proliferation rates normalized to the corresponding control cells in Group I (*left*) and Group II (*right*) diverse human cancer cells with G6PD stable knockdown.

(B) General ROS levels in diverse Group I and Group II human cancer cells with G6PD stable knockdown were measured and compared.

(C) SOD2 mRNA expression level in diverse Group I and Group II human cancer cells was detected by quantitative RT-PCR.

(D) Western blot showing expression level of enzyme related to ROS production and scavenging in diverse Group I and Group II human cancer cells.
(E) Western blot showing expression level of enzyme related to ROS production and scavenging in diverse Group I and Group II human cancer cells with G6PD stable knockdown.
(F) Effect of additional SOD2 transient knockdown on cell proliferation rate and ROS level of H1299 cells with G6PD stable knockdown were detected by cell number counting 96 hours after transfection. Western blot showing the knockdown efficiency.
(G) Effect of SOD2 overexpression on cell proliferation rate and ROS level of WiDr cells with G6PD stable knockdown were detected by cell number counting 96 hours after transfection. Western blot showing protein expression level.
Data are mean ± SD (A, B, C, F and G). *p* values were obtained by a two-tailed Student's *t* test (ns, not significant; *0.01 <p < 0.05; **0.001 < p < 0.01; ***p < 0.001)

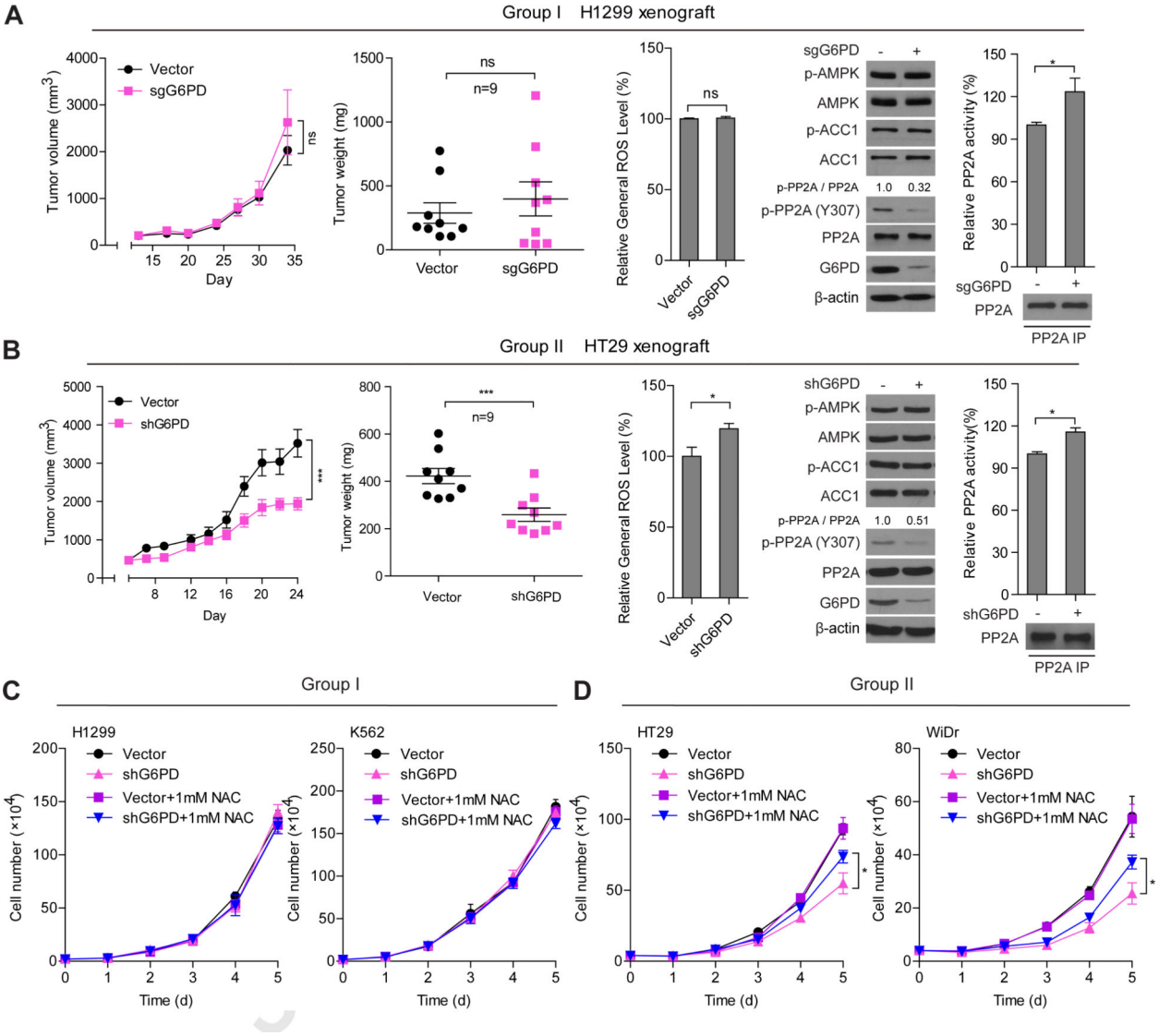

Figure 3. Tumor growth exhibit different pattern upon G6PD attenuation in the two groups of cancer cells.

(A-B) Xenograft tumor growth and tumor weight (*left two panels*), ROS level of xenograft tumor tissue (*middle panel*), Western blot showing AMPK, ACC1 and PP2A phosphorylation, and PP2A enzyme activity of tumor lysates (*right 2 panels*) in nude mice inoculated with Group I H1299 cells (A) and Group II HT29 cells (B) with G6PD CRISPR-knockout.

(C-D) Cell proliferation rates of Group I H1299 and K562 cells (C), and Group II HT29 and WiDr cells (D) with G6PD stable knockdown in the presence or absence of 1mM NAC.

Data are mean ± SD (A-D). *p* values were obtained by a two-tailed Student's *t* test except for a two-way ANOVA test for tumor growth rates (A-B, *left panels*) and cell proliferation rates (D) (ns, not significant; *0.01 < p < 0.05; ***p < 0.001).

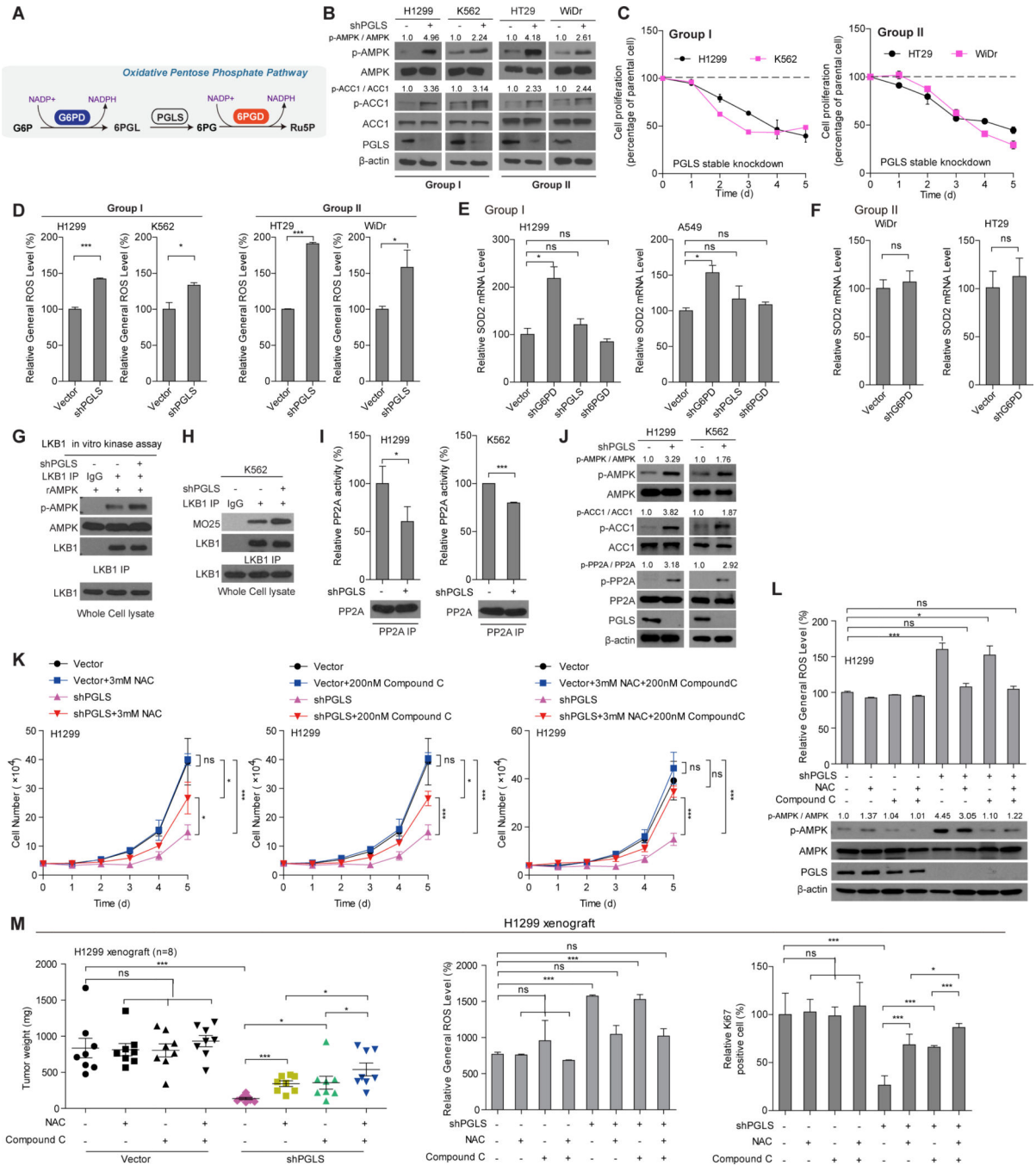

Figure 4. PGLS knockdown inhibits PP2A but activates LKB1, leading to consequent AMPK activation with increased ROS.

(A) Schema showing linear oxidative pentose phosphate pathway with three key enzymes.

(B) Western blot showing effects of PGLS knockdown on AMPK and ACC1 phosphorylation in Group I H1299 and K562 cells and Group II HT29 and WiDr cells.

(C) Corresponding cell proliferation rates in Group I H1299 and K562 cells (*left*) and Group II HT29 and WiDr cells (*right*) with PGLS stable knockdown.

(D) General ROS levels in Group I H1299 and K562 cells (*left*) and Group II HT29 and WiDr cells (*right*) with PGLS stable knockdown.

(E) SOD2 mRNA expression level in H1299 and A549 cells with stable knockdown of G6PD, PGLS, or 6PGD was detected by quantitative RT-PCR.
(F) SOD2 mRNA expression level in WiDr and HT29 cells with G6PD stable knockdown was detected by quantitative RT-PCR.
(G) LKB1 precipitated from K562 cells with or without PGLS knockdown was incubated with rAMPK in an *in vitro* kinase assay. Western blot showing the phosphorylation of AMPK by LKB1.
(H) Western blot showing effect of PGLS knockdown on endogenous LKB1 and MO25 interaction in K562 cells.
(I) Effect of PGLS stable knockdown on PP2A activity in H1299 (*left*) and K562 (*right*) cells.
(J) Western blot showing effects of PGLS stable knockdown on AMPK, ACC1, and PP2A phosphorylation in H1299 (left) and K562 (right) cells.
(K) Cell proliferation rates of H1299 PGLS stable knockdown cells treated with or without 3mM NAC and/or 200nM Compound C.
(L) ROS level (*upper panel*) in H1299 PGLS stable knockdown cells treated with or without 3mM NAC and/or 200nM Compound C was detected. Western blot showing AMPK phosphorylation level (*lower panel*).
(M) NAC (10mg/mL drinking water) and/or Compound C (2 mg/kg, intraperitoneal injection at 4-day intervals) were administrated in H1299 xenograft mice with PGLS knockdown. Tumor weight (*left*), ROS level in tumor cells (*middle*), and quantification of IHC staining signal (*right*) were shown.
Data are mean ± SD (C, D, E, F, I, K, L, and M). *p* values were obtained by a two-tailed Student's *t* test except for a two-way ANOVA test for cell proliferation rates (K) (ns, not significant; *0.01 < p < 0.05; ***p < 0.001).

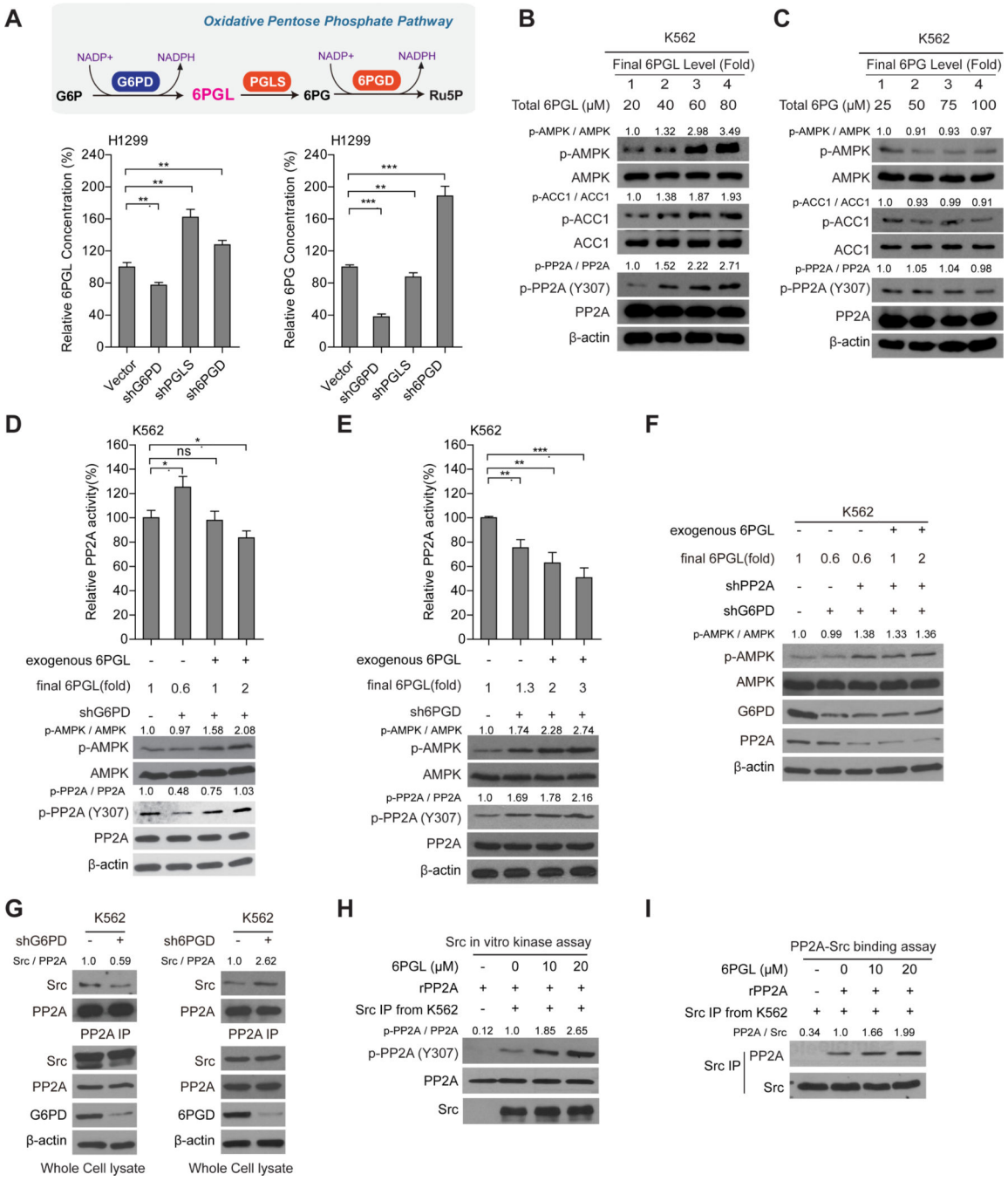

Figure 5. The oxiPPP intermediate 6-phosphogluconolactone (6PGL) enhances inhibitory phosphorylation of PP2A by upstream kinase Src.

(A) Schema of oxidative pentose phosphate pathway (intermediate 6PGL is highlighted) (*upper*). Intracellular level of 6PGL (*lower left*) and 6PG (*lower right*) were measured in H1299 cells with G6PD, PGLS, and 6PGD individually stable knockdown.

(B-C) Effect of 6PGL (B) and 6PG (C) treatment on AMPK, ACC1, and PP2A phosphorylation in K562 cells in a cell-free assay.

(D-E) Cell lysates prepared from G6PD (D) or 6PGD (E) knockdown K562 cells were treated with increasing concentration of 6PGL, followed by detection of PP2A enzyme

activity (*upper panels*) and western blot showing AMPK and PP2A phosphorylation (*lower panels*). Final levels (fold) of 6PGL were normalized to that in control cells without treatment.

(F) Cell lysates from G6PD and PP2A double knockdown K562 cells were treated with increasing concentrations of 6PGL, followed by western blot analysis of AMPK phosphorylation (*upper*). Final levels (fold) of 6PGL were normalized to that in control cells without treatment.

(G) Western blot showing effect of G6PD knockdown (*left*) and 6PGD knockdown (*right*) on endogenous Src and PP2A interaction in K562 cells.

(H- I) Src precipitated from K562 cells was incubated with recombinant PP2A (rPP2A) as substrate in the presence of increasing concentrations of 6PGL in an *in vitro* kinase assay. PP2A phosphorylation (H) and PP2A-Src interaction (I) were detected using western blot. Data are mean ± SD (A and D). *p* values were obtained by a two-tailed Student's *t* test (ns, not significant, *0.01 < p < 0.05; **0.001 < p < 0.01; ***p < 0.001;).

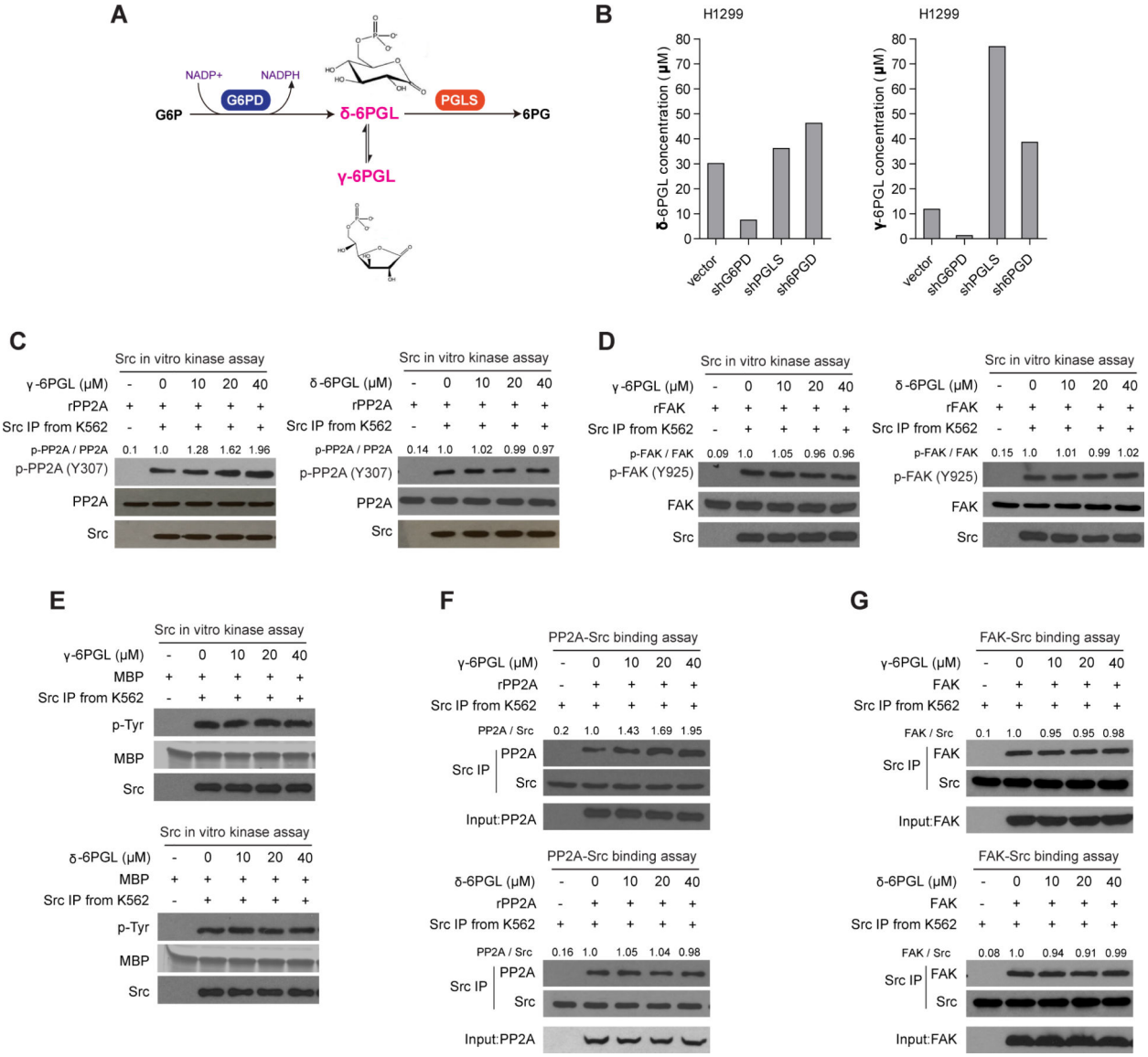

Figure 6. OxiPPP byproduct γ-6PGL enhances the inhibition of PP2A by Src.

(A) Schema for the first two steps of the oxidative pentose phosphate pathway. G6P is catalyzed by G6PD to produce δ-6PGL, which is spontaneously exchanged for γ-6PGL through intramolecular rearrangement.

(B) The intracellular concentrations of δ-6PGL and γ-6PGL in H1299 cells with individual knockdown of G6PD, PGLS, and 6PGD were measured by quantitative ^{31}P nuclear magnetic resonance (^{31}PNMR) spectroscopy. Data were shown as one representative result of two independent biological experiments.

(C-D) Src precipitated from K562 cells was incubated with purified rPP2A (C) or with recombinant FAK (rFAK) (D) as substrate in the presence of increasing concentrations of γ-6PGL (*left*) and δ-6PGL (*right*) in an *in vitro* kinase assay. Phosphorylation of PP2A and FAK were detected by western blot.

(E) Src precipitated from K562 cells was incubated with recombinant myelin basic protein (MBP) as substrate in an *in vitro* kinase assay in the presence of increasing concentrations of

γ-6PGL (*upper*) and δ-6PGL (*lower*). Samples were applied to western blot to detect MBP phosphorylation.

(F-G) Src precipitated from K562 cells was incubated with purified rPP2A (F) or recombinant FAK (rFAK) (G) as substrate in the presence of increasing concentrations of γ-6PGL and δ-6PGL in an *in vitro* kinase assay. The interactions between Src and PP2A (F) or Src and FAK (G) were evaluated by western blot.

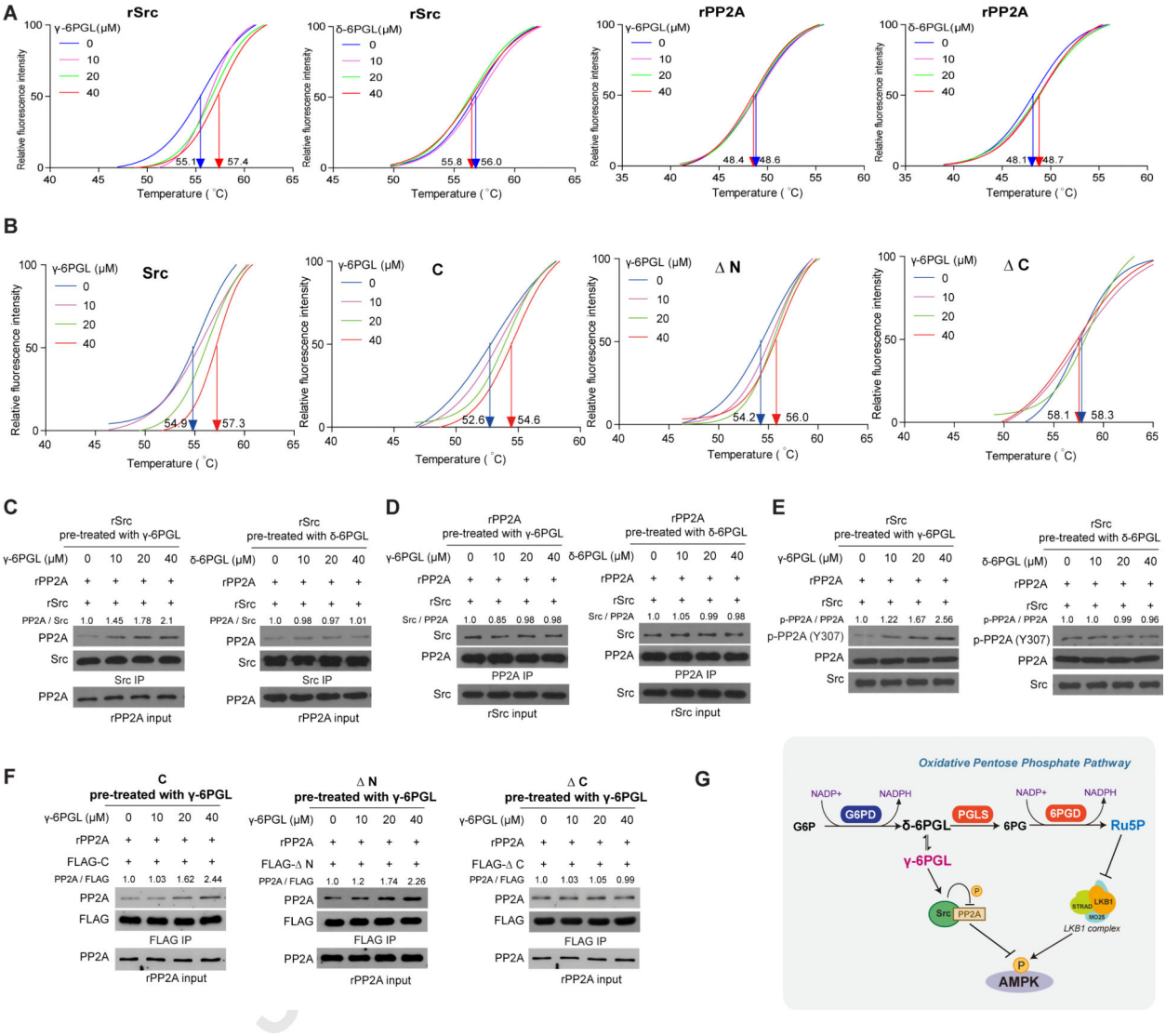

Figure 7. γ-6PGL binds to Src to recruit substrate PP2A.

(A) Thermal melt-shift assay was performed to examine purified recombinant protein Src (rSrc) (*left two panels*) or PP2A (*right two panels*) and ligand (γ-6PGL or δ-6PGL) interaction. Arrows indicate melting temperature at 0 μM and 40 μM.

(B) Thermal melt-shift assay was performed to examine purified recombinant truncated Src domain and ligand γ-6PGL interaction. The full length Src contains amino acids 1–536, the ΔC domain contains amino acids 1–247, the catalytic domain contains amino acids 250–536, and the ΔN domain contains amino acids 88–536. Arrows indicate melting temperature at 0μM and 40μM.

(C) Purified rSrc was pre-treated with increasing concentrations of γ-6PGL (*left*) or δ-6PGL (*right*), followed by incubation with purified rPP2A *in vitro.* Src and PP2A interaction was then detected by western blot.

(D) Purified rPP2A was pre-treated with increasing concentrations of γ-6PGL (*left*) or δ-6PGL (*right*), followed by incubation with purified rSrc protein *in vitro.* Src and PP2A interaction was then detected by western blot.

(E) Purified rSrc was pre-treated with increasing concentrations of γ-6PGL (*left*) or δ-6PGL (*right*), followed by incubation with purified recombinant PP2A *in vitro.* The phosphorylation of PP2A was detected by western blot.
(F) Purified recombinant truncated Src domains, catalytic domain (*left*), ΔN domain (*middle*), and AC domain (*right*), were pre-treated with increasing concentrations of γ-6PGL, followed by incubation with rPP2A *in vitro.* The truncated Src domains and rPP2A interaction were then detected by western blot.
(G) Proposed working model. OxiPPP regulates AMPK homeostasis by balancing the opposing LKB1 and PP2A. The byproduct γ-6PGL converted from δ-6PGL promotes Src-dependent inhibition of PP2A by binding to Src and subsequently enhancing PP2A recruitment, which contributes to AMPK activation.